# Chapter 5

# Stellar temperatures using equivalent width line-ratios

The photometric transit of a planet across the disk of its parent star allows the measurement of the planet to star radius ratio. The measurement of the radial velocity or astrometry wobbles of a star due to an orbiting planet allows the measurement of the planet to star mass ratio. If the stellar radius and mass are precisely measured, the planet radius and mass can be derived more precisely. For bright stars, precise stellar radii can be measured by interferometry or asteroseismology, but for most of the transiting planets, the host stars are not bright enough and other techniques must be used. The most widely used technique, for stars with transiting planets, is to find the stellar evolutionary track corresponding to the density (e.g. $M_s^{1/3}/R_s$) measured from the planetary transit and the stellar temperature measured from the stellar spectrum. Stellar evolution models (e.g. Baraffe et al. 1998, Siess et al. 2000, Girardi et al. 2002) allow us to derive the stellar radius and mass associated to a given stellar atmosphere obtained from comparing the stellar spectrum with stellar atmosphere models (e.g. the ATLAS models, Kurucz 1993).

Precise stellar effective temperatures ($T_{\rm eff}$) are fundamental to many areas in astrophysics, and in particular, to derive precise stellar radii. The $T_{\rm eff}$ of a star can be derived using photometric methods or spectroscopic methods. An example of photometric methods, for bright stars, includes deriving the stellar bolometric flux recovered from multi-band photometry allows us to derive the stellar temperature knowing the stellar radii (see equation 5.1). For instance, the stellar radii can be measured from stellar evolution tracks, interferometry or asteroseismology. Examples of spectroscopic methods include studying the line profile of the H$\alpha$ line, or comparing observed spectra to synthesised spectra from stellar atmosphere models.

Assuming the star radiates as a black body, the stellar luminosity $L$, radius $R_\star$ and effective temperature $T_{\rm eff}$ are related as followed:

$$L = 4\pi R_\star^2 \sigma_{\rm SB} T_{\rm eff}^4 \tag{5.1}$$

where $\sigma_{\rm SB}$ is the Stefan-Boltzmann constant.

Using equation 5.1, the stellar effective temperatures can be derived photometrical, e.g. using temperature calibrated colour bands (e.g. Nordström et al. 2004), spectroscopically, e.g. using $H_\alpha$ wings (e.g. Fuhrmann 1998) or iron lines (e.g. Santos et al. 2004), or through interferometry using the measured stellar radius to derive the stellar temperature. These methods derive uncertainty on the temperature typical down to 80 or 20 K depending on the method and on the star.

This chapter presents a method based on temperature calibrated equivalent width (EW) ratios which allows us to derive stellar relative temperatures with a precision down to 10 K. The current line-ratio temperature calibrations in the literature are based on line depth ratios (e.g. Gray 1994; Kovtyukh et al. 2003). The temperature calibration of equivalent width ratios presented in this chapter are then used to show that such calibration is possible and works well.

After the calibration presented in the chapter was built and tested, an improved version of this calibration was implemented, based on the knowledge gathered from this first calibration. The new calibration is now published in Sousa et al. (2009).

## 5.1 $T_{\rm eff}$ calibration of equivalent width line-ratios

The equivalent width[1] of a spectral line is a measure of the line strength which is sensitive to the temperature (equation 5.2). The ratio of the equivalent widths of two spectral lines can be used as temperature sensors. Each calibrated equivalent width line-ratio can be used to obtain a measurement of the stellar temperature. The larger the number of ratios used, the larger the number of individual measurements of the temperature, which can then be combined together to statistically improve the precision of the stellar temperature.

In Local Thermal Equilibrium (LTE), the ratio of electrons population of two levels $n$ and $m$, i.e. the ratio of the strength of the two spectral lines corresponding to the energy level $n$ and $m$, is:

$$\frac{N_n}{N_m} = \frac{g_n}{g_m}\, e^{-(\chi_n - \chi_m)/kT} \tag{5.2}$$

where $g_n$ and $g_m$ are the statistical weight of level $n$ and $m$ (number of degenerate states at the given energy), $\chi_n$ and $\chi_m$ are the excitation potential (the energy from the ground level) of level $n$ and $m$, $k$ is the Boltzmann constant and, $T$ is the temperature (Gray, 2005).

[1] The equivalent width of a spectral line is the width of a rectangle of length one and an area equal to the area of the spectral line.

### 5.1.1 Choosing the line ratios

The different spectral lines have a different sensitivity to temperature. In this study, the lines are selected and combined into ratios, in order to optimise the response of the line ratios with temperature.

#### Selecting the spectral lines

A list of 268 lines from different chemical elements was computed from Kovtyukh et al. (2003), Kovtyukh (private communication), Santos et al. (2004), and Gilli et al. (2006). The lines used are all located outside telluric absorption lines, and have wavelengths ranging from 5200 to 6800 Å.

Only weak lines (10 mÅ$<$ EW $<$ 200 mÅ in the solar spectrum) were kept, as they are independent of microturbulence and the ratio of such lines show little or no dependence on metallicity variations (Gray, 1994). The lower limit on EWs was set to 10 mÅ as weaker lines are more sensitive to continuum level estimations, as for some sub-solar metallicity, and might not be detectable.

Finally, among the selected lines, only the lines which appear unblended in a high metallicity low temperature stellar spectrum of our sample (HD59686: (Fe/H)=0.28, T=4871 K, Santos et al. 2005) were kept. The criterion for blends was to visually exclude lines overlapped by another line by more than $\sim 5\%$ of their EW. Identifying blended lines in the spectrum of a cool-metal rich star, provides a worse case scenario for blends within our sample of stellar spectra.

Applying the above criteria resulted in a list of 155 spectral lines from different chemical elements with wavelength ranging from 5490 to 6722 Å, excitation potentials ranging from 0.8 to 5.0 eV.

#### Combining the spectral lines into line ratios

To maximise the dependence of the equivalent width line-ratios on temperature and minimise their dependence on other parameters, the 155 selected spectral lines are combined into line ratios following four criteria:

1. Lines close in wavelength are combined into ratios. The continuum level is the same for these lines and will cancel out in the ratio of the lines, minimising the influence of the uncertainty on the continuum evaluation in the equivalent width line-ratios. Here lines within $70$ Å from each other were combined together (value used in Kovtyukh et al. 2003).

2. Lines with large differences in excitation potential were combined. Lines with high excitation potential will be highly responsive to any temperature variations. Combining them with lines of low excitation potentials (low response to temperature variations) will give ratios to build ratios highly sensitive to temperature variations.

Here, lines with excitation potential difference greater than $3\,eV$ were combined together.

3. Lines from different chemical elements are combined into ratios. The electronic population of the energy levels of a single chemical element can be dependent on other effects than the temperature (e.g. in NLTE[2] where the relative strength of the lines of a chemical element is dependent on the density of the medium), in which case combining lines from the same element will avoid this.

4. Lines from chemical elements with the same or similar behaviour of abundance ratio $[\mathrm{X/Fe}]$ with metallicity $[\mathrm{Fe/H}]$ are combined into ratios, to avoid a dependence of the ratios on metallicity. The calibration stars have different metallicities, and among the sample, the chemical elements – which EW are combined into ratios – should have a similar response of relative abundances with metallicity. The chemical elements are classified into 5 categories, according to the variation of their abundance ratio $[\mathrm{X/Fe}]$ with metallicity (Gilli et al., 2006). FeI, MgI, SiI and TiI are classified as abundance ratio constant with metallicity, VI, AlI, NaI, NiI as abundance ratio weakly increasing with metallicity, CaI as abundance ratio weakly decreasing with metallicity, CoI and MnI have as abundance ratio strongly increasing with metallicity.

Applying these criteria returned 278 line ratios (Table 5.6) built with 116 spectral lines (Table 5.3) from 8 different chemical elements.

### 5.1.2 Calibrating the line ratios with temperature

The selected line ratios need to be temperature calibrated. This is done using a set of calibration stars as described below .

#### The calibration stars

The starting set of stars used to calibrate the equivalent width line-ratios with temperature, is composed of 101 stars with a high resolution and high signal-to-noise ratio (200-400) spectrum. The spectra of 50 of the stars were taken with UVES[3] and the spectra of the 51 other stars with FEROS[4]. Using high resolution spectra allows a more accurate measurement of the equivalent widths. The stars are solar-type (F-K) with temperature ranging from 4500 to 6200 K, metallicity (Fe/H) from $-0.5$ to $0.5$, and $\log g$ from 2.5 to 4.7. Their temperatures are taken from Santos et al. (2004), Santos et al. (2005) and

[2]NLTE = Non Local Thermodynamic Equilibrium, which happens when the density of the medium is low enough that the dominant mode of energy transport becomes radiation and not collisions.

[3]UVES: echelle spectrograph with a maximum resolution of 100000, mounted on the VLT/UT2 8m Kueyen Telescope at ESO Paranal Observatory, Chile.

[4]FEROS: 100000-resolution echelle spectrograph on the 2.2m Telescope in ESO La Silla Observatory, Chile.

Sousa et al. (2006). These authors all used the same technique to derive the stellar parameters and provide a set of calibration temperature homogeneously determined which allows us to minimise the scatter in temperature within each line ratios. The stellar temperature derived in these papers were obtained using the line abundance code $\mathrm{MOOG}$[5]. MOOG uses ATLAS9 (Kurucz, 1993) stellar atmosphere models to create model spectra. These models are compared to the equivalent widths measured on the observed stellar spectrum, and with a condition on the Fe ionisation balance MOOG returns the stellar atmospheric parameters ($T_{\rm eff}$, $\log(g)$, metallicity (Fe/H), and microturbulence) corresponding to the data.

The spectra used in this work are the same as the ones used in Santos et al. (2004), Santos et al. (2005) and Sousa et al. (2006). They were pre-reduced by these authors using UVES and FEROS reduction pipelines.

### Measuring the equivalent widths with $\mathrm{ARES}$

A standard method to measure the equivalent width of a spectral line is to use an interactive routine – such as $\mathrm{IRAF}$ – where the continuum position is fitted by eye for each individual line. In this case, the measurement has an intrinsic human error that is difficult to estimate. Using an automatic process to measure the equivalent width reduces the human error. In this chapter, the equivalent widths are measured using the software $\mathrm{ARES}$[6] (Sousa et al., 2007) which measures the equivalent width of an input list of absorption spectral lines for a given parameter list and a given stellar spectrum. $\mathrm{ARES}$ currently does not return uncertainties on the measured equivalent widths; this suggestion has been sent to the author and should be implemented in a future version of the software. Using a Linux script, this software is run automatically over the 101 stellar spectra of the data set to measure the equivalent width of the 116 selected spectral lines in each spectrum. The 278 equivalent width line-ratios are then computed for each star using an $\mathrm{IDL}$ code.

$\mathrm{ARES}$ has a list of input parameters. The $rejt$ parameter determines the points in the spectrum used to evaluate the local continuum. This parameter needs to be adjusted according to the signal to noise ratio ($S/N$) of each spectrum (see Sousa et al. (2008) for a table of correspondence between the $S/N$ and the optimal $rejt$). To keep the equivalent width measurements as automated as possible, and because in our data set the different spectra obtained from the same spectrograph have a similar S/N, a single value of $rejt$ is adopted for each spectrograph (0.998 for the UVES spectra and 0.990 for the FEROS spectra). Sousa et al. (2009) discusses on the effect of the $rejt$ value on the derived temperature using temperature calibrated equivalent width line-ratios similar to the one presented in this chapter. The $smoothder$ parameter corresponds to the width (in pixels) of the boxcar used to reduce the noise in the spectra and allow

[5]http://verdi.as.utexas.edu/moog.html
[6]http://www.astro.up.pt/ sousasag/ares/

a better fit of the lines. The $space$ parameter sets the wavelength range used on each side of the lines to evaluate the local continuums. The $lineresol$ parameter defines the minimum separation (in Å) between consecutive lines. The $miniline$ parameter sets the lower value of the equivalent width returned by ARES. The default values used here are $smoothder = 4$, $space = 3$, $lineresol = 0.1$, and $miniline = 2$.

The number of stars with successfully measured equivalent width ratios varies for each line ratio, depending on whether ARES successfully measured the equivalent width of the two spectral lines of the ratio. If a star is visually far from the other stars (e.g. more than $4\sigma$) when plotted in an equivalent width ratio – e.g. due to a line miss-measured by ARES or affected by a cosmic ray) – the star is removed from the sample of calibration stars. After this selection, 62 stars are left to calibrate the line ratios (Figure 5.1).

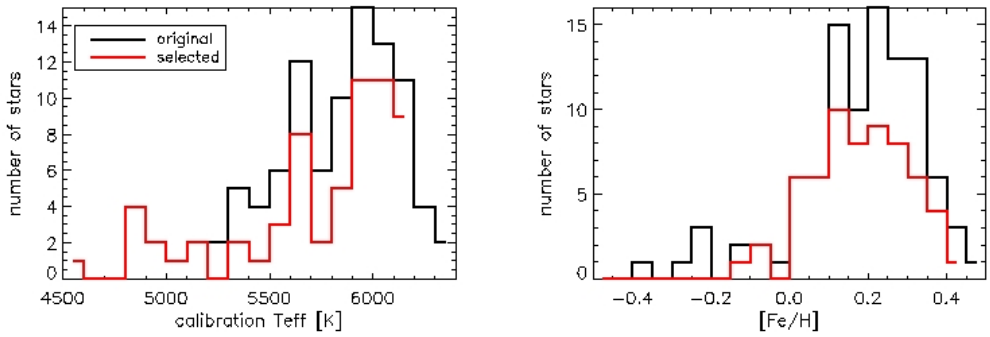


Figure 5.1: Distribution in temperature (left) and metallicity (right) of the 62 calibration stars (red) and the original sample of 101 stars (black).

### Fitting function

For each of the 278 line ratios, the dependence of the equivalent width line-ratios $r^{j}_{\rm EW}$ with the stellar effective temperatures $T^{S,j}_{\rm eff}$ ($j$ for each calibration star, $S$ for calibration temperature taken from Santos et al. (2004), Santos et al. (2005) and Sousa et al. (2006)) was fitted with a $3^{rd}$ order polynomial function. For each line ratio, a best fit is derived with the POLYFIT function of IDL[7], weighing each data points ($r^{j}_{\rm EW}$,$T^{S,j}_{\rm eff}$) with the uncertainty on the $T^{S,j}_{\rm eff}$.

The equivalent width ratios are calibrated against temperature as follows:

$$T^{S,j}_{\rm eff} = c_0 + c_1\, r^{i,j}_{\rm EW} + c_2\, {r^{i,j}_{\rm EW}}^{2} + c_3\, {r^{i,j}_{\rm EW}}^{3} \tag{5.3}$$

where $c_0$, $c_1$, $c_2$ and $c_3$ are respectively the zeroth, first, second and third order of the $3^{rd}$ order polynomial function, and $i$ is the line ratio.

[7]IDL: Interactive Data Language

### Selection of the final calibration set

For each line ratios, the standard deviation of the points around the best fit is calculated and taken as the uncertainty in temperature of the calibration of this ratio. The uncertainties on the individual calibrations ranges from 30 K to 240 K.

To minimise the uncertainties on the final temperature $T_{\rm eff}^{f}$ derived from the calibrated line ratios, the first 68% of the ratios with the lowest standard deviation from the fit are selected, which corresponds to standard deviation less than 100 K. This selection resulted in 190 ratios, composed of 88 spectral lines.

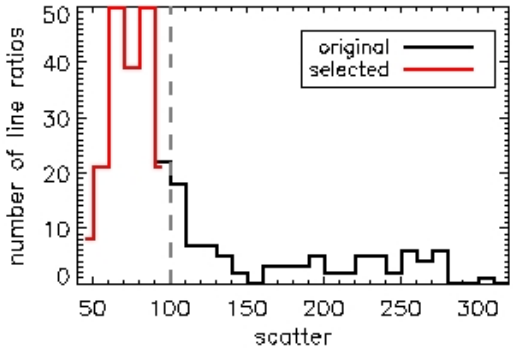


Figure 5.2: Distribution in standard deviation of the equivalent width line-ratios calibrated in temperature. The 278 original line ratios are plotted in black and the 190 selected line ratios in red. The 100 K limit in standard deviation, used for the selection, is marked by the dashed line.

## 5.1.3 Using the calibration to derive stellar temperatures

In a spectrum, the equivalent width of a spectral line can be inaccurately measured (e.g. due to line blends or cosmic rays affecting the determination of the local continuum). This will affect the value derived for the associated line ratio and return a wrong $T_{\rm eff}^{k}$ for this ratio. This temperature is classified as an "outlier" and to avoid taking it into account in the final temperature $T_{\rm eff}^{f}$, a $2\sigma$ clipping from the median of the $T_{\rm eff}^{k}$s (equation 5.8) is applied, where $\sigma$ is the 1.48*MAD[8] of the $T_{\rm eff}^{k}$s (equation 5.9).

There are several ways to combine the remaining individual temperature measurements into a final temperature. The weighted average of the measurements (equation 5.4, and equation 5.5 for the associated uncertainty) can be used when the accuracy of the individual measurements (values and uncertainties) can be trusted. The mean of the measurements (equation 5.6, and equation 5.7 for the associated uncertainty) can be used when the exactitude of the individual measurements can be trusted but not the associated uncertainties. The median of the measurements (equa-

[8]MAD: Median Absolute Deviation

tion 5.8, and equation 5.9 for the associated uncertainties) can be used when the exactitude of the individual measurements (values and uncertainties) cannot be trusted.

As the outlying temperatures have already been removed, the final temperature can be obtained by taking the mean of the remaining individual measurements of the temperature (equation 5.6, and equation 5.7 for the uncertainty). The weighted mean is not used as it is not certain that the uncertainties associated to the individual temperature take into account all the sources of uncertainties.

Weighted average:

$$T_{\text{eff}}^{f} = \frac{\sum_k \frac{T_{\text{eff}}^{k}}{\sigma_k{}^2}}{\sum_k \frac{1}{\sigma_k{}^2}} \tag{5.4}$$

where $\sigma_k$ is the uncertainty on the individual measurement of temperature ($T_{\text{eff}}^{k}$) for the line ratio $k$. The uncertainty associated to the weighted average is

$$\sigma_{T_{\text{eff}}^{f}} = \frac{1}{\sum_k \frac{1}{\sigma_k{}^2}} \tag{5.5}$$

Mean:

$$T_{\text{eff}}^{f} = \frac{\sum_k T_{\text{eff}}^{k}}{N} \tag{5.6}$$

where $N$ is the number of individual measurements of temperature combined together. The uncertainty associated to the mean is

$$\sigma_{T_{\text{eff}}^{f}} = \sqrt{\frac{\sum_k (T_{\text{eff}}^{k} - T_{\text{eff}}^{f})^2}{N}} \; \frac{1}{\sqrt{N_i}} \tag{5.7}$$

where $N_i$ is the number of independent measurements of the temperature. In this work the number of independent measurements is taken as the number of unique combinations of chemical elements into line ratios. It is not taken as the total number of line ratios as several ratios are made of the same combination of elements and are therefore not independent from each other.

Median:

$$T_{\text{eff}}^{f} = T_{\text{eff}}^{k}|_{k=med} \tag{5.8}$$

When ordering the $T_{\text{eff}}^{k}$, $med$ is the index of the $T_{\text{eff}}^{k}$ with as many individual temperatures larger than $T_{\text{eff}}^{med}$ than smaller. The uncertainty associated to the median is

$$\sigma_{T_{\text{eff}}^{f}} = 1.48 * |T_{\text{eff}}^{k} - T_{\text{eff}}^{f}|_{k=med} \; \frac{1}{\sqrt{N_i}} \tag{5.9}$$

### 5.1.4 Testing the calibration

To evaluate the performance of the equivalent width line-ratio calibration set built in the previous sections, the three following tests were performed:

#### The inverse test

The first test is an inverse experiment where the 62 stars used to build the calibration are run back into the calibration and the resulting temperatures are compared to the values used to build the calibration. If the calibration is working well, both sets of temperature should be consistent within the error bars.

The resulting temperatures are plotted versus the original ones in Figure 5.3. For the stars with calibration temperature between 5000 and 6100 K, there is a good agreement between the calibration $T_{\rm eff}$ and the equivalent width $T_{\rm eff}$. But for the stars with calibration temperature lower than 5000 K, the current calibration overestimates the $T_{\rm eff}$ by up to 200 K, and for the stars with calibration temperature larger than 6100 K, the current calibration underestimates the $T_{\rm eff}$ by up to 100 K.

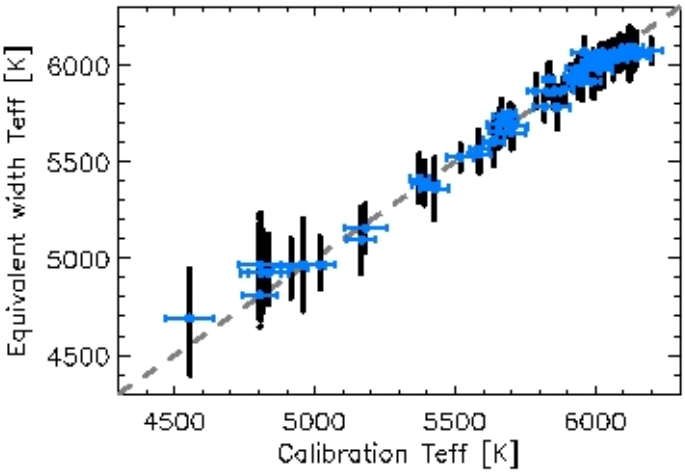


Figure 5.3: In blue, the $T_{\rm eff}$ of the 62 calibration stars derived using the equivalent width line-ratio calibration (y-axis), compared to the value of their $T_{\rm eff}$ with error bars used to build the calibration (x-axis). For each star (x-axis), the black dots along the y-axis are the $T_{\rm eff}$ measured from the individual line-ratios. The equivalent width $T_{\rm eff}$ and the associated error bars (along the y-axis, in blue) are derived as described in section 5.1.3. The grey dashed line is the identity line between the calibration $T_{\rm eff}$ and the equivalent width $T_{\rm eff}$.

#### Test on lower resolution spectra

The second test evaluates the performance of the calibration when using a spectrum with a resolution smaller than that of the spectra used to build the calibration.

The equivalent width line-ratio calibration is run on four stars with 50000-resolution spectra taken with CORALIE [9]. These spectra were reduced in Santos et al. (2004) using the standard tasks in the IRAF echelle package. The spectra have an $S/N$ of about 190 so the equivalent width are measured with ARES using $rejt = 0.992$. The individual $T_{\rm eff}$ derived from each calibrated equivalent width line-ratios are presented in Figure 5.4. The final $T_{\rm eff}$, derived as described in section 5.1.3, are compared in Table 5.1 to the value in Santos et al. (2004).

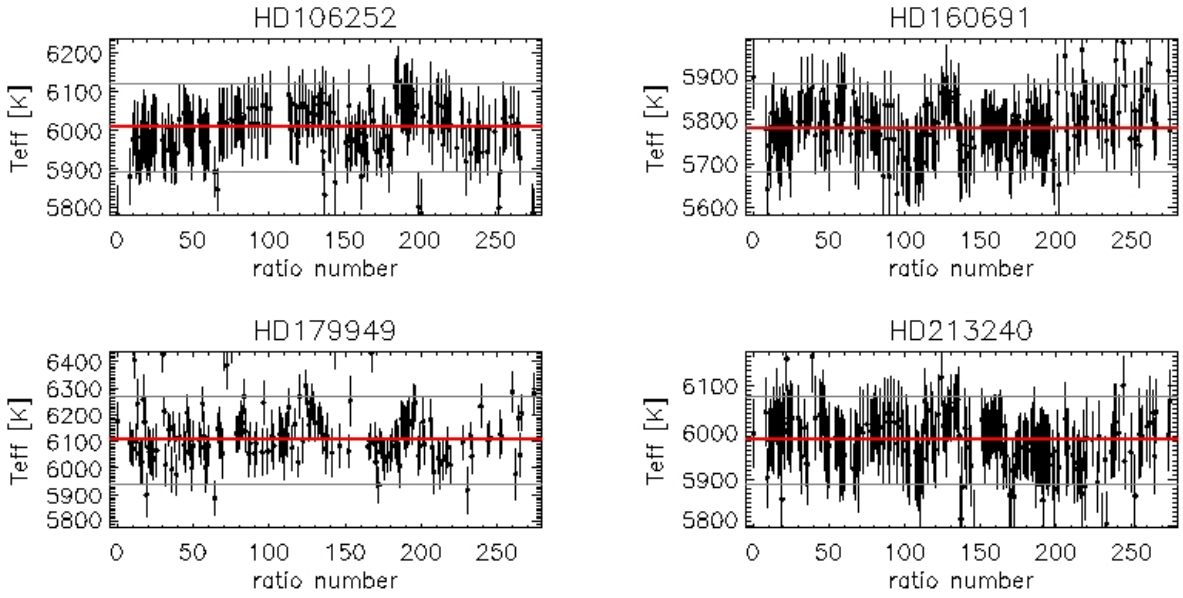


Figure 5.4: Test of the equivalent width line-ratio calibration on four stars with CORALIE spectra. Each point marks the $T_{\rm eff}$ and its uncertainty derived with the corresponding equivalent width line-ratio (numbered on the x-axis). The grey lines marks the levels at plus and minus twice the scatter from the median of the individual $T_{\rm eff}$, outside which the individual $T_{\rm eff}$ are considered as outliers. The red line marks the final $T_{\rm eff}$ derived as the mean of the $T_{\rm eff}$ within the grey lines.

Table 5.1: $T_{\rm eff}$ derived using the equivalent width calibration on the CORALIE spectra, compared to the values obtained by Santos et al. (2004) on the same spectra. $N_r$ is the number of ratios used to compute the final $T_{\rm eff}$, $N_i$ is the number of independent ratio, used to derive the uncertainty on the $T_{\rm eff}$, taken as the number of unique combinations of chemical elements in the line ratios.

| | This Chapter | | | Santos et al. (2004) |
|---|---|---|---|---|
| | $T_{\rm eff}$ | $N_r$ | $N_i$ | $T_{\rm eff}$ |
| HD106252 | 6009±14 | 159 | 11 | 5899±35 |
| HD160691 | 5782±13 | 177 | 12 | 5798±33 |
| HD179949 | 6111±20 | 139 | 12 | 6260±43 |
| HD213240 | 5986±11 | 168 | 12 | 5984±33 |

[9] CORALIE: 50000-resolution spectrograph on the 1.2m Euler Swiss Telescope at the ESO La Silla Observatory, Chile

For the two cooler stars, the final $T_{\rm eff}$ derived is consistent within the error bars with Santos et al. (2004), while the uncertainties derived with the equivalent width line-ratio calibration are smaller (half) than those from Santos et al. (2004). The two hotter stars have derived $T_{\rm eff}$ 110 and 150 K different from the value cited in Santos et al. (2004). For the star with $T_{\rm eff}$>6100 K, the underestimation of the temperature by the equivalent width line-ratio calibration was also identified in the previous test. The mis-match in temperature for the other star is not understood.

This test shows that the equivalent width measurements with $\rm ARES$ and the method used to combine the individual $T_{\rm eff}$ return consistent temperatures even for lower resolution spectra, as long as the temperature is within the temperature range where the calibration performs well ((5000,6100) K as defined in the previous test).

#### Test stars at various $rejt$

The $rejt$ parameter is used in $\rm ARES$ to select which points of the spectrum are used to evaluate the local continuum. This parameter is dependent on the signal to noise ratio of the spectrum. To keep the procedure automated, and as all the spectra used to calibrate the equivalent width line-ratios have similar $S/N$ (200-400), a unique $rejt$ is used for all the UVES spectra (0.998) and for all the FEROS spectra (0.990). For S/N varying from 200 to 400, the $rejt$ value should vary from 0.993 to 0.996. To evaluate the effect on the temperature derived from the equivalent width line-ratio calibration, of a $rejt$ value not optimised to the $S/N$ of the spectrum, the following test is performed. Three stars ($T_{\rm eff}$=4810, 5699, 6143 K), with similar (Fe/H) and spectra taken with the same spectrograph (UVES), the equivalent widths are measured for $rejt$ ranging from 0.990 to 0.999. The $T_{\rm eff}$ is derived for each of the $rejt$ value using the equivalent width line-ratio calibration. An additional star ($T_{\rm eff}$=5696 K) with a similar metallicity which has a spectrum taken with FEROS is studied in the same way. Figure 5.5 plots the resulting $T_{\rm eff}$ versus the value of $rejt$.

Figure 5.5 shows that the stellar $T_{\rm eff}$ can vary by 12 to 25 K depending on the $rejt$ value used to measure the equivalent widths. Within the explored range of $rejt$, the $T_{\rm eff}$ of the three UVES stars remain different to the value in Santos et al. (2004) by 30 to 100 K. The $T_{\rm eff}$ for the FEROS star is consistent with Santos et al. (2004).

This test indicates that choosing a $rejt$ value not optimised to the spectrum, introduces an additional uncertainty in the final $T_{\rm eff}$. To take this into account, an uncertainty of $\sim$25 K – coming from the uncertainty of the equivalent width measurements – should be added in quadrature. To reduce this additional source of uncertainty, the $rejt$ parameter should be adjusted for each spectrum. This is not aways straight forward as even a small difference (e.g. 0.001) in $rejt$ results in a difference of 5 to 10 K in the final $T_{\rm eff}$.

The unique values of $rejt$ used for the UVES and the FEROS calibration spectra can explain the large number of calibration stars (21 UVES, 18 FEROS) that were dropped

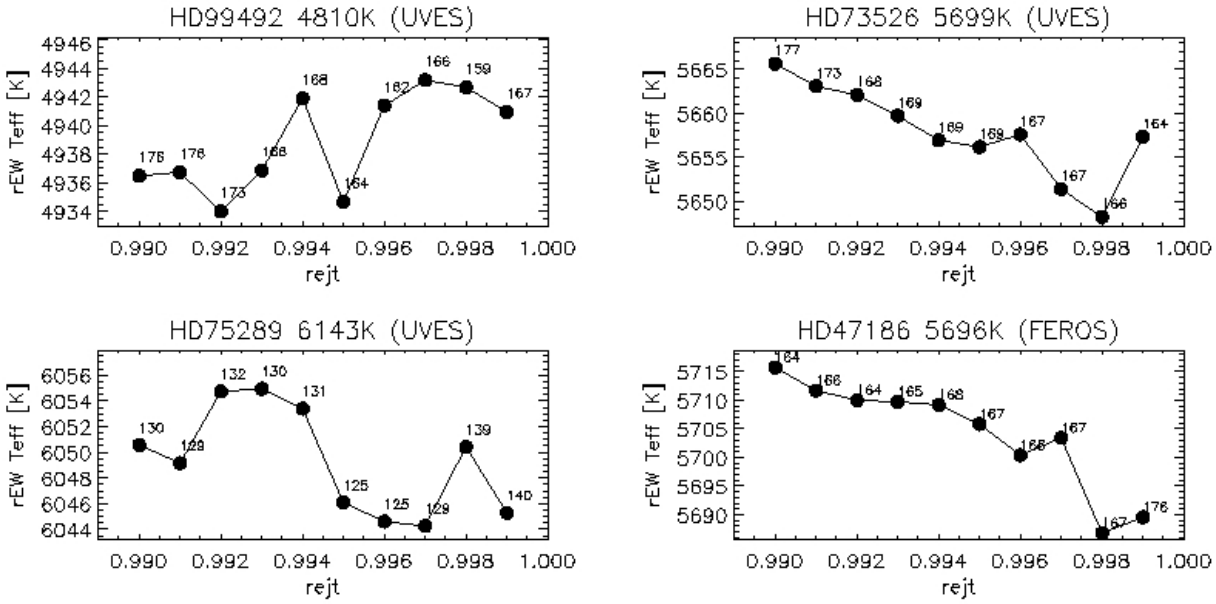


Figure 5.5: $T_{\rm eff}$ derived from the equivalent width line-ratio calibration, versus the $rejt$ value used to measure the EWs. The $T_{\rm eff}$ as derived by Santos et al. (2004) is indicated above each plot. The number of equivalent width line-ratios used to derive the $T_{\rm eff}$ in each $rejt$ trial is indicated in small prints by the side of each point.

out of the calibration sample as their equivalent width line-ratio $T_{\rm eff}$ were outliers.

This test shows on how the choice of $rejt$ value when measuring the EWs with $\rm ARES$ impacts the $T_{\rm eff}$ derived with the equivalent width line-ratio calibration.

### 5.1.5 Discussion

This section summarises the strengths and limitations of the equivalent width line-ratio calibration. It then lists some suggestions to improve this calibration.

#### Strengths

The calibration presented in this chapter is composed of 190 equivalent width line ratios calibrated for temperatures ranging from $4500\,K$ to $6200\,K$., with equivalent width measured uniformly using $\rm ARES$ and calibration temperature derived uniformly by previous authors.

This calibration is the first to present such a large number of calibrated equivalent width ratios. It was developed further and published in Sousa et al. (2009). Previous works on this subject calibrated line-depth ratios, not equivalent width ratios, and published less ratios (e.g. Kovtyukh et al. (2003) published 105 calibrations of line-depth ratios). This calibration demonstrates that equivalent width ratios are as good as line-depth ratios to measure stellar temperatures, contrarily to previous believes that they would not be precise enough as they are more sensitive to blends.

With its large number of calibrated line ratios, this calibration allows temperatures to be to derived with smaller relative uncertainties. The calibration was tested on 4 stars and, within the error bars, the temperatures are consistent with Santos et al. (2004), while our relative temperature error bars are at least a factor of two smaller.

The calibration can be applied to the monitoring of stellar variation in temperature, e.g. due to spots. From an exoplanet point of view, this could be used to tell apart spots mimicking planetary transits from real planetary transits (e.g. Biazzo et al. 2006).

### Limitations

The calibration is valid only over the calibrated temperature range (4500 to 6200 K), and loses precision below 5000 K and above 6100 K.

Only a temperature relative to another measurement, with the same calibration, can be determined with a better precision. The absolute temperature suffers from the same systematic offsets in temperature as the sample of calibration stars (e.g. $\sim$10 K compared to Ramírez & Meléndez 2004 as derived in Santos et al. 2005). In the case of exoplanets, to derive an accurate and precise stellar radius, one needs an accurate and precise stellar temperatures. The calibration of equivalent width line ratios is thus limited when it comes to deriving absolute temperature.

The accuracy on the $T_{\rm eff}$ is also dependent on that of the equivalent width measurements. For instance, the equivalent widths measured with $\rm ARES$ have an uncertainty due to the continuum determination controlled by the $rejt$, which is difficult to optimise for each spectrum. This uncertainty translates into $\sim$25 K in temperature, and needs to be added in quadrature to the uncertainty from the calibration itself – derived as the scatter in the individual $T_{\rm eff}$ measured). When using another tool to measure the equivalent widths, the user should evaluate and propagate the uncertainty on their equivalent width measurements to the final $T_{\rm eff}$.

### Improvements

The calibration can be improved by having more calibration stars. The 59 stars removed from the calibration sample can be revisited with adjusted $rejt$ to derive better equivalent widths and thus better values of the equivalent width line-ratios for these stars. Also, for a given star, if only some of the equivalent width line-ratio measurements are outliers, the star can be selectively removed from the affected ratios instead of systematically from the whole calibration.

The sample of stars can also be extended to lower $T_{\rm eff}$ to improve the quality of the calibration in that temperature range. The sample can also be extended outside the current calibration range in order to extend the temperature range over which the calibration can be applied.

The quality of the calibration can be in general improved with more precise measurements of equivalent widths, e.g. by using a $rejt$ value adapted to each spectrum.

The choice in fitting function used to model the dependence of the equivalent width with temperature can be diversified, e.g. by adding the functions $\frac{1}{x}$ and $\log x$ to the $3^{rd}$ order polynomial functions, and by selecting the function modelling each ratio with the smallest residuals.

The number of spectral lines can be increased, by widening the wavelength range or by changing the criteria of selection of good line ratios (e.g. loosening the 100 K limit in standard deviation). This will increase the number of line ratios, and thus theoretically improve the precision on the derived $T_{\rm eff}$. Adding spectral lines at shorter wavelength will improve the determination of the $T_{\rm eff}$ of hotter stars which have less lines at longer wavelengths.

In practice they are sources of uncertainty on the derived $T_{\rm eff}$ (e.g. from the $\rm ARES$ parameter $rejt$, or from the calibration temperatures) that should be taken into account when associating an uncertainty to an absolute temperature. These other sources of uncertainties are larger than the precision achieved by the current calibration. Thus, developing a more precise calibration (large number of ratios, fitting function, accuracy of the EWs measurements) will not make a major difference on the uncertainties associated with the absolute temperature.

## 5.2 Comparison to the calibration of Sousa et al. (2009)

An improved version of the calibration described in the previous sections, taking into account most of the points mentioned in Section 5.1.5, was published in Sousa et al. (2009).

In this new calibration, a larger number of calibration stars (451) are used, all with high resolution HARPS spectra (R$\sim$110000), with 90% of the spectra with a $S/N > 200$, and with calibration temperatures homogeneously derived in Sousa et al. (2008). The sample of calibration stars covers more uniformly the (4500,6500) K range.

This calibration is composed of a larger number of equivalent width line ratios. The initial line list was extended to 498 spectral lines. The spectra lines were combined into ratios only on the basis of their proximity in wavelength ($<$ 70 Å) and their difference in excitation potential $>$ 3 eV). The equivalent width measurements were obtained with $\rm ARES$ adjusting the $rejt$ parameter for each spectra. Ratios with a very weak and/or a very strong spectral line were removed as the equivalent width measured for these lines can be affected by the continuum estimate (for the weak lines) or by the gaussian fit to the line (for the strong lines).

In Sousa et al. (2009), the best fit to each equivalent width line-ratio $r$, calibrated in temperature ($T_{\rm eff}$), is selected among 6 models: a linear fit and a $3^r d$ order polynomial fit to the relations ($T_{\rm eff}$ vs. $r$), ($T_{\rm eff}$ vs. $1/r$) and ($T_{\rm eff}$ vs. $\log r$). Finally, only the equivalent

width line-ratios measured in more than 300 stars and with a standard deviation to the best temperature calibration fit smaller than 120 K, were kept. Based on these criteria, the calibration published in Sousa et al. (2009) is composed of 433 line ratios built with 171 spectral lines.

In Sousa et al. (2009), the final temperature is derived as the weighted average of the temperatures from the individual equivalent with ratios, after having removed those temperatures outside the (4200,6800) K range and the ones outside a $2\sigma$ range from the average temperature. The uncertainty associated to this final temperature is derived as the standard deviation of the individual temperatures used to derived the final temperature, divided by the square root of the number of independent line ratios (i.e. the number of line ratios with unique combination of chemical elements). Sousa et al. (2009) published a correction function to the final temperature, to be applied if the temperature derived is greater than 6000 K.

The calibration derived in Sousa et al. (2009) is applied to the 62 calibration stars used to build the calibration presented in this chapter. The $T_{\rm eff}$ are plotted in Figure 5.6 and compared to the value derived with the calibration presented in this chapter.

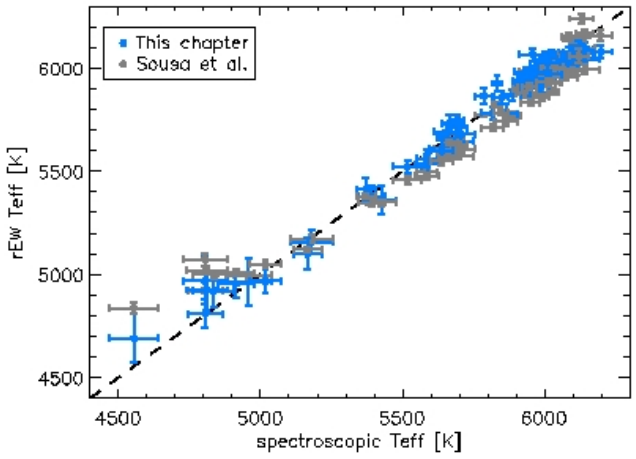


Figure 5.6: The $T_{\rm eff}$ derived with the calibration presented in this chapter (blue) versus the $T_{\rm eff}$ derived with the calibration presented in Sousa et al. (2009) (grey), for the 62 calibration stars used to build the calibration presented in this chapter. The dashed line is the identity line between the spectroscopic $T_{\rm eff}$ and the equivalent width ratio $T_{\rm eff}$.

The $T_{\rm eff}$ derived by the two calibrations are consistent within the errors bars. In general, the $T_{\rm eff}$ from Sousa et al. (2009) calibration have smaller error bars than the $T_{\rm eff}$ from the calibration described in this chapter. For the high $T_{\rm eff}$ stars, the calibration of Sousa et al. (2009) derives a $T_{\rm eff}$ closer to the identity line than this chapter's calibration, due to the systematic temperature correction applied to the high $T_{\rm eff}$ stars in the calibration of Sousa et al. (2009). For the low $T_{\rm eff}$ stars, this chapter's calibration derives $T_{\rm eff}$ slightly closer to the identity line than the calibration of Sousa et al. (2009). The difference observed between the two calibrations, is likely due to the approach

used when combining the individual $T_{\rm eff}$, as Sousa et al. (2009) derive the final $T_{\rm eff}$ as the weighted average which is more sensitive to wrong measurements of equivalent width line-ratio associated to line-ratios with small internal errors.

## 5.3 Applying the calibration to the host stars of CoRoT planets

In this section, the effective temperature $T_{\rm eff}$ of the host stars of the planets CoRoT-1b to 9b, are derived using the temperature calibrated equivalent width line-ratio technique. Two calibration sets and methods to combine the individual $T_{\rm eff}$ are used: the calibration set described in this chapter and the calibration set derived in Sousa et al. (2009), and re-described in section 5.2.

### 5.3.1 Spectra and equivalent width measurements

The spectra used in this section are UVES spectra for CoRoT-1,2,3,6,8,9 and HARPS spectra for CoRoT-4,5,7. The spectra are the same as the ones used for the determination of the stellar parameters in the discovery papers of the associated orbital companion. The UVES and HARPS spectra were reduced prior to this work with the standard instrument pipelines. Additionally, as the HARPS spectra were originally taken to measure the variations in radial velocity due to the orbital companion; after correcting each order of the spectra from its blaze function, the spectra were weight averaged order per order according to their $S/N$, to increase the $S/N$ of the spectrum used to derive the stellar atmosphere parameters.

In this work, the following additional reduction steps were performed on the spectra using the IRAF software: 1) the spectra were normalised order per order using the CONTINUUM task and the spline function of order 3 to 5, 2) the orders were merged using the SCOMBINE task, and 3) the stellar radial velocity was corrected, when needed, using the DOPCOR task.

The list of spectral lines used in the calibration presented in this chapter and in the calibration by Sousa et al. (2009) are combined into a single line list which is inputed into ARES to uniformly measure the equivalent width of all the spectral lines and avoid biases in equivalent width measurements between the two calibrations. The default ARES parameters used are $smoothder = 4$, $space = 3$, $lineresol = 0.15$ and $miniline = 2$. The values of $space$ and $lineresol$ have been slightly increased to account for the slighly noisier spectra compared to the spectra used to built the calibration presented in this chapter.

The $S/N$ of the different spectra vary from 40 to 240 so the $rejt$ parameter is adjusted for each spectrum. For the UVES spectra (CoRoT-1,2,6,8), the $S/N$ can vary from 70 to 180 across a single spectrum due to the level of fringing in the redder part of the spectrum which increases the noise in this range. For these spectra a single $rejt$ value

(0.990) is used to compromise between the different values of the $S/N$. The spectrum of CoRoT-4,5,9 have smaller $S/N$ (70, 50 and 90 respectively) so smaller values of $rejt$ are used (0.989, 0.985 and 0.989 respectively). The spectrum of CoRoT-7 has a larger $S/N$ (150-240) so a larger $rejt$ is used (0.993). For CoRoT-3, the spectral lines are broad, so the values used for $lineresol$ and $space = 8$ are increased to 0.4 and 8 respectively. These parameters set the minimum resolution between consecutive spectral lines and the wavelength range around the spectral lines used to evaluate the continuum. The value of both needs to be larger for broader lines.

### 5.3.2 Deriving the effective temperatures

The measured equivalent widths of each star are run through the calibrated equivalent width line-ratios described in this chapter. Figure 5.7 shows the individual $T_{\rm eff}$ derived from each ratio and the value of the combined $T_{\rm eff}$ (red line).

The measured equivalent widths are then run through the calibration of Sousa et al. (2009), also described in section 5.2, and the corresponding $T_{\rm eff}$ are extracted. If the derived $T_{\rm eff}$ is larger than 6000 K, a temperature correction is applied as described in Sousa et al. (2009). For CoRoT-6, the $T_{\rm eff}$ was corrected by -10 K.

The $T_{\rm eff}$ of the host stars of CoRoT-1b to 9b, derived from the two calibration sets, are presented in Table 5.2, along with the number of ratios used in each case and the value of the $T_{\rm eff}$ taken from the discovery paper.

Table 5.2: $T_{\rm eff}$ of CoRoT 1b to 9b derived using the two sets of equivalent width ratio calibrations, compared to the value in the literature. $N_r$ is the number of ratios used to compute the $T_{\rm eff}$, $N_i$ the number of independent ratios used to derive the uncertainty.

| | This chapter | | | Sousa et al. (2009) | | | Literature | |
|---|---|---|---|---|---|---|---|---|
| | $T_{\rm eff}$ | $N_r$ | $N_i$ | $T_{\rm eff}$ | $N_r$ | $N_i$ | $T_{\rm eff}$ | Ref. |
| CoRoT-1 | 6015±35 | 131 | 11 | 5919±77 | 264 | 19 | 5950±150 | Barge et al. (2008) |
| CoRoT-2 | 5663±50 | 163 | 12 | 5516±33 | 325 | 20 | 5625±120 | Alonso et al. (2008) |
| CoRoT-3 | 5974±84 | 66 | 11 | 5856±100 | 111 | 14 | 6740±140 | Triaud et al. (2009) |
| CoRoT-4 | 5971±46 | 158 | 12 | 5927±60 | 324 | 23 | 6190±60 | Aigrain et al. (2008) |
| CoRoT-5 | 5832±56 | 161 | 12 | 5736±66 | 333 | 22 | 6100±65 | Rauer et al. (2009) |
| CoRoT-6 | 6069±44 | 113 | 11 | 6014±73 | 184 | 16 | 6090±70 | Fridlund et al. (2010) |
| CoRoT-7 | 5333±34 | 181 | 12 | 5291±9 | 383 | 29 | 5275±75 | Léger et al. (2009) |
| CoRoT-8 | 5122±46 | 163 | 12 | 5134±40 | 354 | 20 | 5150±75 | Bordé et al. (2010) |
| CoRoT-9 | 5741±44 | 161 | 12 | 5563±35 | 331 | 18 | 5625±80 | Deeg et al. (2010) |

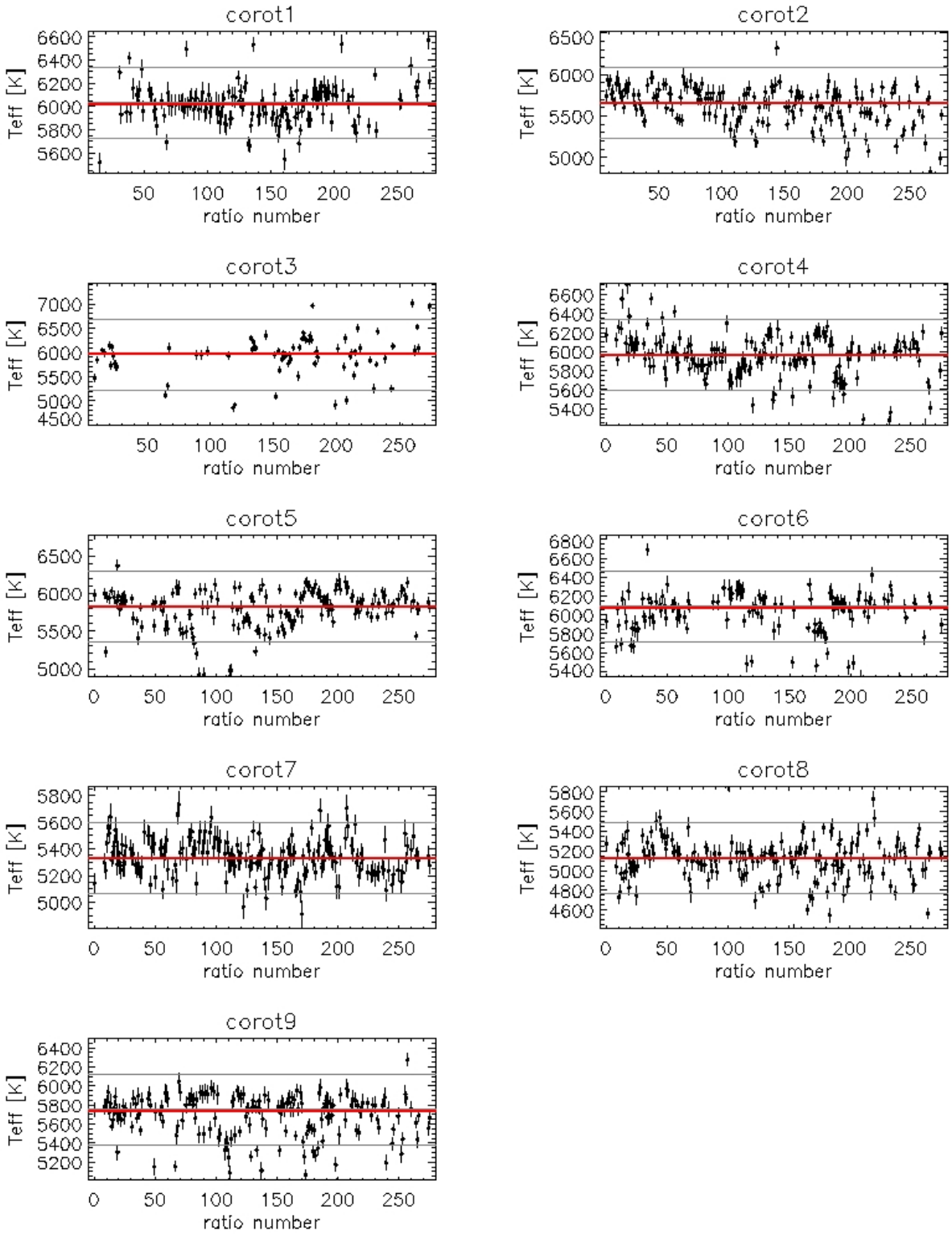


Figure 5.7: The $T_{\rm eff}$ of the CoRoT planet host stars derived from the equivalent width line-ratio calibration described in this chapter, based on UVES spectra for CoRoT-1,2,3,6,8,9 and HAPRS spectra for CoRoT-4,5,7. Same legend as Figure 5.4.

### 5.3.3 Discussion

The $T_{\rm eff}$ of the CoRoT planet host stars derived with the equivalent width line-ratios technique (both calibration set) are consistent within the error bars with the stellar $T_{\rm eff}$ published in the discovery papers, except for CoRoT-3,4,5. The uncertainties derived using the equivalent with ratios technique are in general smaller than those from the discovery papers (expect for CoRoT-4,5,6) when using the calibration set of Sousa et al. (2009).

The values of the $T_{\rm eff}$ derived from the calibration of this chapter are consistent within the error bars with those derived from the calibration of Sousa et al. (2009), except for CoRoT-2 and 9. The uncertainties derived with the calibration described in this chapter are smaller than those derived with the calibration of Sousa et al. (2009), except for CoRoT-2,7,8,9.

For CoRoT-2 and 9, the values of $T_{\rm eff}$ derived with the calibration set described in this chapter are 70 and 100 K higher than the values of $T_{\rm eff}$ derived with the calibration of Sousa et al. (2009). The reason for this difference is unclear as the $T_{\rm eff}$ are well within the calibrated temperature range of the two calibration sets, and as the equivalent widths of all the spectral lines were measured uniformly and should return uniform line ratios and thus uniform $T_{\rm eff}$. A possible difference could be in the approach used to combine the individual $T_{\rm eff}$. The weighted average used by Sousa et al. (2009) is more sensitive to outlier equivalent width measurements associated to well calibrated line ratios. This could explain the $T_{\rm eff}$ derived with the calibration of Sousa et al. (2009) but not the $T_{\rm eff}$ derived with the calibration of this chapter as the latter uses normal averaging of the individual $T_{\rm eff}$.

CoRoT-3 is a hot and fast rotating star, therefore its spectrum has less lines in the visible, and the spectral lines are broad so more likely to be blended. This results in fewer line ratios well measured by $\rm ARES$, which in turn limits the accuracy of the $T_{\rm eff}$ derived from the temperature calibrated equivalent width line-ratios. For this star, the $T_{\rm eff}$ of the two calibration sets are consistent with each other, which is as expected given the equivalent widths of the two sets were measured at the same time. But these $T_{\rm eff}$ are not consistent with the value in the discovery paper because the temperature of the star is outside the temperature range calibrated.

The $T_{\rm eff}$ of CoRoT-3,4,5, derived from equivalent width ratios, are underestimated. Their $T_{\rm eff}$ are larger than 6100 K, temperatures above which the calibration derived in this chapter are known to underestimate the $T_{\rm eff}$, as seen in section 5.1.4. The calibration of Sousa et al. (2009) has a correction function at $T_{\rm eff}>$6000 K, integrated into the derivation of the final $T_{\rm eff}$, but for these CoRoT host stars, the $T_{\rm eff}$ derived by the calibration is smaller than 6000 K, so the correction is not applied.

## 5.4 Conclusion

The equivalent width line ratios calibrated against temperature, is a successful method to derive stellar effective temperature, within the temperature calibrated range, and using medium to high resolution (R>50000) and signal-to-noise ($S/N$ >40) spectra.

The limitation to the precision of the $T_{\rm eff}$ derived with this method is not in the number of line ratios used but in the precision of the equivalent width measurements and local continuum. Using softwares (such as $\rm ARES$) to automatically measure the equivalent width of a large number of spectral lines makes the derivation of the $T_{\rm eff}$ faster and removes biases due to human "eye-ball" intervention in line fitting (such as with $\rm IRAF$), but the derived equivalent width measurements largely depend on the input parameters (such as $rejt$ in $\rm ARES$) which introduces an additional source of uncertainties in the derived $T_{\rm eff}$.

The equivalent width line ratio technique was applied to the host stars of CoRoT-1b to 9b and the derived $T_{\rm eff}$ are consistent with the discovery papers, except for the stars hotter than 6100 K. The associated uncertainties derived purely from the combination of the individual temperatures are smaller than the uncertainties published in the discovery papers, but are highly sensitive to the $\rm ARES$ $rejt$ value chosen.

The two sets of equivalent width line ratios presented in this chapter combine the individual $T_{\rm eff}$ differently. A larger and more uniform calibration set than the one presented in this chapter was developed in Sousa et al. (2009). Although the $T_{\rm eff}$ derived with the two calibrations are consistent, the calibration of Sousa et al. (2009) is an improvement to the calibration presented in this chapter. Thus, the $T_{\rm eff}$ and uncertainties kept for CoRoT-1b to 9b are those derived from the calibration of Sousa et al. (2009).

This chapter has presented an alternative method to measure the stellar temperature from the stellar spectrum. The $T_{\rm eff}$ derived with this method provides an additional measurement to compare with the values from the other methods, and increase or reduce the confidence on the value of the stellar temperature. The method presented here also has the advantages of been fast, automated and homogeneous, even if, like for the other methods, the temperature scale is not absolute.

# 5.5 Appendix

## 5.5.1 Line list

Table 5.3: List of the 116 spectral lines in the 278 lines ratios identified in section 5.1.2, with $\lambda$ the wavelength, $EP$ (Excitation Potential) the energy of the level above the ground state, $\log gf$ the weighted oscillator strength (product of the oscillator strength $f$ of the atomic transition and the statistical weight $g$ of the lower level), and $A$ the atomic number of the chemical element. The values of $EP$ and and $\log gf$ are taken from the VALD atomic database (Piskunov et al., 1995).

| $\lambda$ | $EP$ | $\log gf$ | $\lambda$ | $EP$ | $\log gf$ | $\lambda$ | $EP$ | $\log gf$ |
|---|---|---|---|---|---|---|---|---|
| **NaI (A = 11)** | | | 6090.21 | 1.081 | -0.150 | 6200.32 | 2.608 | -2.437 |
| 5688.22 | 2.104 | -0.625 | 6111.65 | 1.043 | -0.715 | 6213.43 | 2.223 | -2.482 |
| 6154.23 | 2.102 | -1.607 | 6135.36 | 1.051 | -0.746 | 6215.15 | 4.186 | -1.320 |
| 6160.75 | 2.104 | -1.316 | 6216.35 | 0.280 | -0.900 | 6226.73 | 3.880 | -2.066 |
| **MgI (A = 12)** | | | 6251.82 | 0.287 | -1.340 | 6232.65 | 3.654 | -1.223 |
| 5711.09 | 4.346 | -1.706 | **CrI (A = 24)** | | | 6240.66 | 2.223 | -3.233 |
| 6318.72 | 5.108 | -1.996 | 6330.13 | 0.941 | -2.920 | 6246.32 | 3.602 | -0.733 |
| **SiI (A = 14)** | | | **FeI (A = 26)** | | | 6252.55 | 2.404 | -1.687 |
| 5517.53 | 5.082 | -2.384 | 5619.60 | 4.386 | -1.700 | 6254.26 | 2.279 | -2.443 |
| 5621.60 | 5.082 | -2.500 | 5633.97 | 4.991 | -0.270 | 6265.13 | 2.176 | -2.550 |
| 5690.43 | 4.930 | -1.790 | 5650.71 | 5.085 | -0.960 | 6271.29 | 3.332 | -2.703 |
| 5701.11 | 4.930 | -2.020 | 5651.47 | 4.473 | -2.000 | 6330.86 | 4.733 | -1.740 |
| 5753.65 | 5.616 | -0.830 | 5662.52 | 4.178 | -0.573 | 6380.75 | 4.190 | -1.321 |
| 5772.15 | 5.082 | -1.620 | 5680.26 | 4.186 | -2.580 | 6392.55 | 2.280 | -3.932 |
| 5948.55 | 5.080 | -1.110 | 5701.54 | 2.559 | -2.216 | 6592.91 | 2.727 | -1.473 |
| 6125.03 | 5.610 | -1.520 | 5705.99 | 4.607 | -0.530 | 6608.03 | 2.279 | -4.030 |
| 6142.49 | 5.619 | -1.480 | 5717.85 | 4.284 | -1.130 | 6609.12 | 2.559 | -2.692 |
| 6145.02 | 5.616 | -1.480 | 5731.77 | 4.256 | -1.300 | 6627.56 | 4.548 | -1.680 |
| 6155.14 | 5.619 | -0.750 | 5753.12 | 4.260 | -0.688 | 6677.99 | 2.692 | -1.418 |
| 6237.33 | 5.614 | -0.530 | 5852.23 | 4.550 | -1.187 | 6703.58 | 2.758 | -3.160 |
| 6244.48 | 5.616 | -0.690 | 5855.08 | 4.610 | -1.529 | 6710.33 | 1.485 | -4.880 |
| 6414.99 | 5.871 | -1.100 | 5856.09 | 4.290 | -1.564 | 6750.15 | 2.424 | -2.621 |
| 6583.71 | 5.954 | -1.640 | 5862.36 | 4.549 | -0.058 | **NiI (A = 28)** | | |
| 6721.85 | 5.863 | -1.090 | 5956.70 | 0.859 | -4.605 | 5578.72 | 1.676 | -2.650 |
| **ScII (A = 21)** | | | 5983.69 | 4.549 | -1.878 | 5587.86 | 1.930 | -2.380 |
| 5526.82 | 1.770 | 0.150 | 5987.05 | 4.795 | -0.556 | 5682.20 | 4.100 | -0.390 |
| 6245.62 | 1.510 | -1.040 | 6007.96 | 4.652 | -0.966 | 5754.68 | 1.935 | -2.330 |
| 6604.60 | 1.360 | -1.160 | 6027.06 | 4.080 | -1.180 | 6007.31 | 1.676 | -3.330 |
| **TiI (A = 22)** | | | 6055.99 | 4.733 | -0.460 | 6086.29 | 4.266 | -0.440 |
| 5490.15 | 1.460 | -0.980 | 6056.01 | 4.730 | -0.498 | 6108.12 | 1.676 | -2.450 |
| 5866.45 | 1.070 | -0.840 | 6065.48 | 2.608 | -1.530 | 6111.07 | 4.090 | -0.800 |
| 6091.18 | 2.267 | -0.460 | 6078.50 | 4.795 | -0.424 | 6128.99 | 1.680 | -3.370 |
| 6126.22 | 1.067 | -1.410 | 6089.57 | 4.580 | -3.112 | 6130.14 | 4.260 | -0.950 |
| 6258.11 | 1.440 | -0.440 | 6098.28 | 4.558 | -1.880 | 6175.42 | 4.089 | -0.559 |
| 6261.11 | 1.430 | -0.490 | 6102.18 | 4.835 | -0.627 | 6176.81 | 4.088 | -0.260 |
| **VI (A = 23)** | | | 6105.15 | 4.548 | -2.050 | 6186.74 | 4.105 | -0.960 |
| 5670.85 | 1.081 | -0.460 | 6127.91 | 4.143 | -1.399 | 6204.64 | 4.088 | -1.100 |
| 5703.59 | 1.051 | -0.211 | 6151.62 | 2.176 | -3.299 | 6223.99 | 4.105 | -0.910 |
| 5727.05 | 1.080 | -0.000 | 6157.73 | 4.070 | -1.240 | 6327.60 | 1.676 | -3.150 |
| 5737.07 | 1.060 | -0.770 | 6159.38 | 4.610 | -1.860 | 6586.33 | 1.951 | -2.810 |
| 6039.73 | 1.064 | -0.650 | 6165.37 | 4.140 | -1.503 | 6767.77 | 1.826 | -2.170 |
| 6081.44 | 1.051 | -0.579 | 6188.00 | 3.940 | -1.631 | | | |

### 5.5.2 List of the calibration stars

Table 5.4: List of the final 62 calibration stars used to calibrate the line ratios, as described in section 5.1.2. The stellar parameters were taken from Santos et al. (2004), Santos et al. (2005) and Sousa et al. (2006).

| star | $T_{\rm eff}$ $(K)$ | (Fe/H) | $\log g$ $(cms^{-2})$ | | star | $T_{\rm eff}$ $(K)$ | (Fe/H) | $\log g$ $(cms^{-2})$ | |
|---|---|---|---|---|---|---|---|---|---|
| HD4203 | 5636±40 | 0.40±0.05 | 4.23±0.14 | (1) | HD73256 | 5518±49 | 0.26±0.06 | 4.42±0.12 | (1) |
| HD7199 | 5426±52 | 0.39±0.06 | 4.41±0.07 | (2) | HD73524 | 6012±50 | 0.23±0.06 | 4.40±0.03 | (2) |
| HD7570 | 6198±39 | 0.24±0.05 | 4.44±0.09 | (1) | HD73526 | 5699±49 | 0.27±0.06 | 4.27±0.12 | (1) |
| HD7727 | 6131±41 | 0.16±0.05 | 4.34±0.02 | (2) | HD74156 | 6112±39 | 0.16±0.05 | 4.34±0.10 | (1) |
| HD8326 | 4914±63 | 0.10±0.07 | 4.30±0.11 | (2) | HD75289 | 6143±53 | 0.28±0.07 | 4.42±0.13 | (1) |
| HD9562 | 5937±36 | 0.26±0.05 | 4.13±0.02 | (2) | HD78429 | 5786±31 | 0.11±0.05 | 4.34±0.02 | (2) |
| HD9782 | 6023±36 | 0.15±0.05 | 4.40±0.02 | (2) | HD82943 | 6028±19 | 0.29±0.02 | 4.45±0.07 | (1) |
| HD81110A | 5818±38 | 0.31±0.05 | 4.50±0.03 | (2) | HD99492 | 4810±72 | 0.26±0.07 | 4.21±0.21 | (1) |
| HD10180 | 5912±24 | 0.13±0.04 | 4.33±0.01 | (2) | HD102117 | 5708±46 | 0.33±0.06 | 4.31±0.09 | (2) |
| HD11226 | 6099±32 | 0.09±0.04 | 4.31±0.01 | (2) | HD114386 | 4834±77 | -0.06±0.06 | 4.33±0.29 | (1) |
| HD11964A | 5372±35 | 0.14±0.05 | 3.99±0.04 | (2) | HD117618 | 6013±41 | 0.06±0.06 | 4.39±0.07 | (1) |
| HD13043A | 5934±21 | 0.14±0.03 | 4.33±0.01 | (2) | HD121504 | 6075±40 | 0.16±0.05 | 4.64±0.12 | (1) |
| HD19994 | 6121±33 | 0.19±0.05 | 4.19±0.12 | (1) | HD128311 | 4835±72 | 0.03±0.07 | 4.44±0.21 | (1) |
| HD20201 | 6064±34 | 0.19±0.05 | 4.43±0.02 | (2) | HD177565 | 5664±28 | 0.14±0.04 | 4.43±0.09 | (2) |
| HD23079 | 5959±46 | -0.11±0.06 | 4.35±0.12 | (1) | HD177830 | 4804±77 | 0.33±0.09 | 3.57±0.17 | (1) |
| HD28185 | 5656±44 | 0.22±0.05 | 4.44±0.05 | (1) | HD183263 | 5991±28 | 0.34±0.04 | 4.38±0.17 | (2) |
| HD33214 | 5180±74 | 0.17±0.08 | 4.40±0.11 | (2) | HD183658 | 5833±19 | 0.08±0.03 | 4.42±0.01 | (2) |
| HD33636B | 6046±49 | -0.08±0.06 | 4.71±0.09 | (1) | HD190248 | 5638±40 | 0.39±0.05 | 4.33±0.04 | (2) |
| HD37605 | 5391±49 | 0.31±0.06 | 4.37±0.18 | (2) | HD190360A | 5584±36 | 0.24±0.05 | 4.37±0.06 | (1) |
| HD37986 | 5586±42 | 0.35±0.05 | 4.38±0.05 | (2) | HD192310 | 5166±52 | 0.04±0.06 | 4.39±0.08 | (2) |
| HD39091 | 5991±27 | 0.10±0.04 | 4.43±0.07 | (1) | HD199190 | 5946±25 | 0.20±0.04 | 4.25±0.01 | (2) |
| HD43745 | 6086±28 | 0.14±0.04 | 3.98±0.01 | (2) | HD204385 | 6022±24 | 0.09±0.04 | 4.31±0.01 | (2) |
| HD47186 | 5696±29 | 0.27±0.04 | 4.39±0.03 | (2) | HD208487 | 6141±29 | 0.06±0.04 | 4.52±0.15 | (2) |
| HD47536 | 4554±85 | -0.54±0.12 | 2.48±0.23 | (1) | HD209458 | 6117±26 | 0.02±0.03 | 4.48±0.08 | (1) |
| HD50554 | 6026±30 | 0.01±0.04 | 4.41±0.13 | (1) | HD213240 | 5984±33 | 0.17±0.05 | 4.25±0.10 | (1) |
| HD52265 | 6103±52 | 0.20±0.07 | 4.27±0.15 | (1) | HD216435 | 5938±42 | 0.24±0.05 | 4.12±0.05 | (1) |
| HD55693 | 5951±34 | 0.32±0.04 | 4.41±0.02 | (2) | HD216437 | 5887±32 | 0.25±0.04 | 4.30±0.07 | (1) |
| HD61606 | 4958±80 | 0.01±0.08 | 4.45±0.19 | (2) | HD221420 | 5864±43 | 0.37±0.06 | 4.06±0.03 | (2) |
| HD66221 | 5655±33 | 0.21±0.05 | 4.39±0.03 | (2) | HD222480 | 5848±24 | 0.21±0.04 | 4.20±0.01 | (2) |
| HD70642 | 5693±26 | 0.18±0.04 | 4.40±0.15 | (1) | HD224022 | 6134±46 | 0.15±0.06 | 4.30±0.02 | (2) |
| HD72659 | 5995±45 | 0.03±0.06 | 4.30±0.07 | (1) | HD330075 | 5017±53 | 0.08±0.06 | 4.22±0.11 | (1) |

(1) = UVES spectrum
(2) = FEROS spectrum

### 5.5.3 Plot of the line ratio and their calibration

Table 5.5: Plot of the 190 equivalent width line-ratios calibrated against temperature, with the $3^{rd}$ order polynomial function (coefficients in Table 5.6) modelling the dependency of the ratios with temperature (red line). Each dot is a calibration star with its $T_{\rm eff}$ taken from Santos et al. (2004), Santos et al. (2005) or Sousa et al. (2006), and its equivalent width is measured with $\rm ARES$. "sdev" is the scatter of the points.

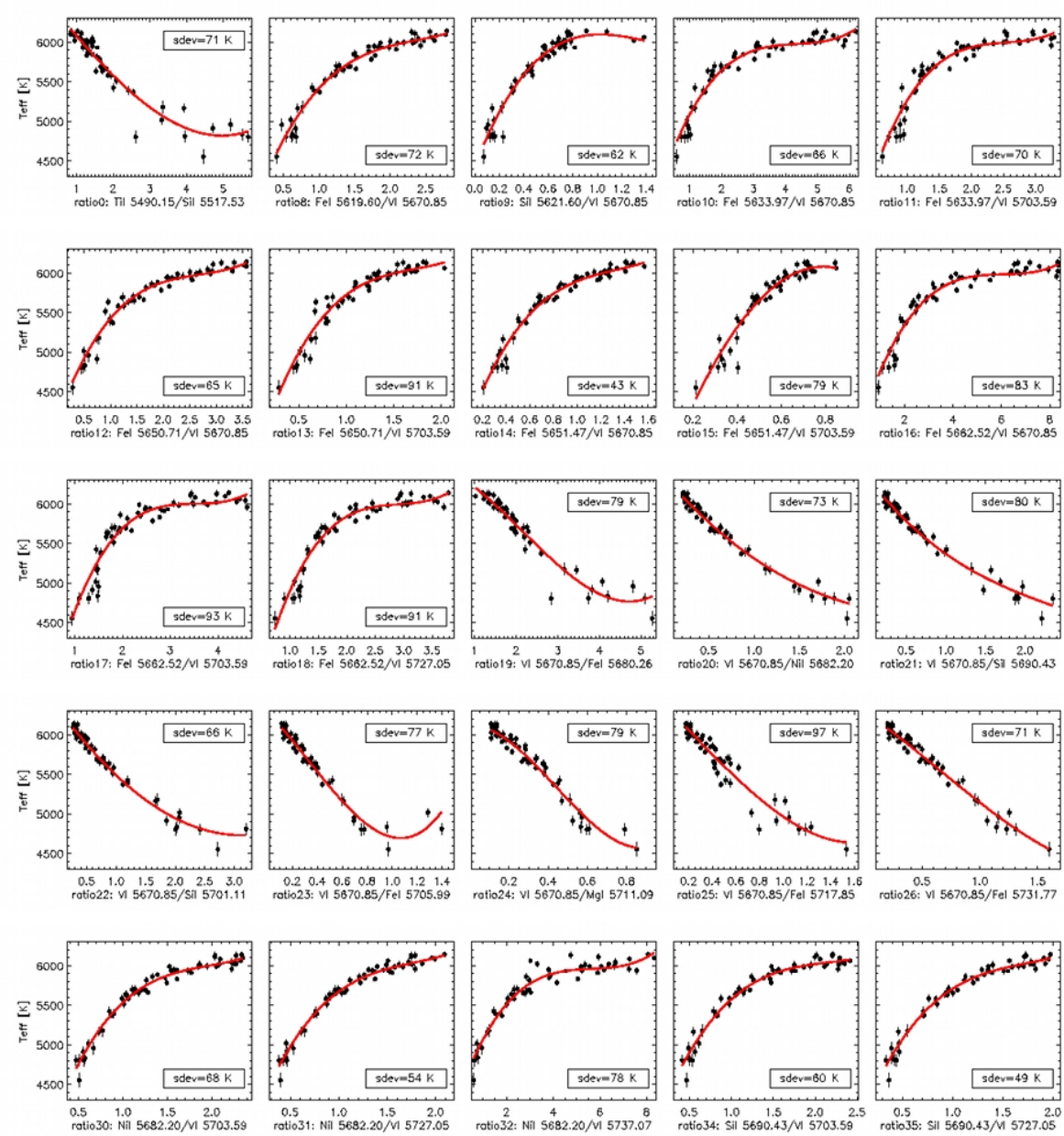

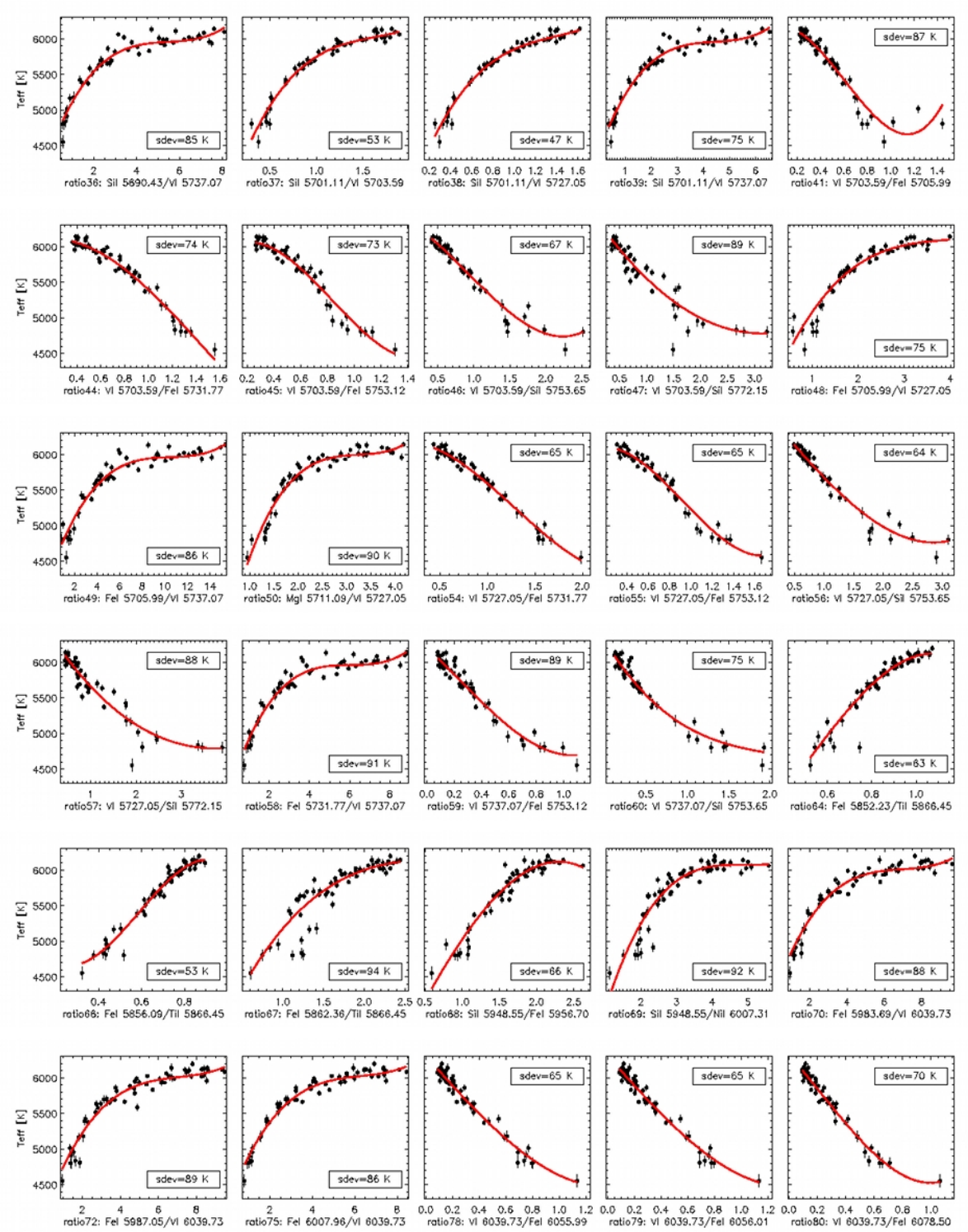
Teff [K]
sdev=85 K
ratio36: SiI 5890.43/VI 5737.07
sdev=53 K
ratio37: SiI 5701.11/VI 5703.59
sdev=47 K
ratio38: SiI 5701.11/VI 5727.05
sdev=75 K
ratio39: SiI 5701.11/VI 5737.07
sdev=87 K
ratio41: VI 5703.59/FeI 5705.99
sdev=74 K
ratio44: VI 5703.59/FeI 5731.77
sdev=73 K
ratio45: VI 5703.59/FeI 5753.12
sdev=67 K
ratio46: VI 5703.59/SiI 5753.65
sdev=89 K
ratio47: VI 5703.59/SiI 5772.15
sdev=75 K
ratio48: FeI 5705.99/VI 5727.05
sdev=86 K
ratio49: FeI 5705.99/VI 5737.07
sdev=90 K
ratio50: MgI 5711.09/VI 5727.05
sdev=65 K
ratio54: VI 5727.05/FeI 5731.77
sdev=65 K
ratio55: VI 5727.05/FeI 5753.12
sdev=64 K
ratio56: VI 5727.05/SiI 5753.65
sdev=88 K
ratio57: VI 5727.05/SiI 5772.15
sdev=91 K
ratio58: FeI 5731.77/VI 5737.07
sdev=89 K
ratio59: VI 5737.07/FeI 5753.12
sdev=75 K
ratio60: VI 5737.07/SiI 5753.65
sdev=83 K
ratio64: FeI 5852.23/TiI 5866.45
sdev=53 K
ratio66: FeI 5856.09/TiI 5866.45
sdev=94 K
ratio67: FeI 5862.36/TiI 5866.45
sdev=66 K
ratio68: SiI 5948.55/FeI 5956.70
sdev=92 K
ratio69: SiI 5948.55/NiI 6007.31
sdev=88 K
ratio70: FeI 5983.69/VI 6039.73
sdev=89 K
ratio72: FeI 5987.05/VI 6039.73
sdev=86 K
ratio75: FeI 6007.96/VI 6039.73
sdev=65 K
ratio78: VI 6039.73/FeI 6055.99
sdev=65 K
ratio79: VI 6039.73/FeI 6056.01
sdev=70 K
ratio80: VI 6039.73/FeI 6078.50

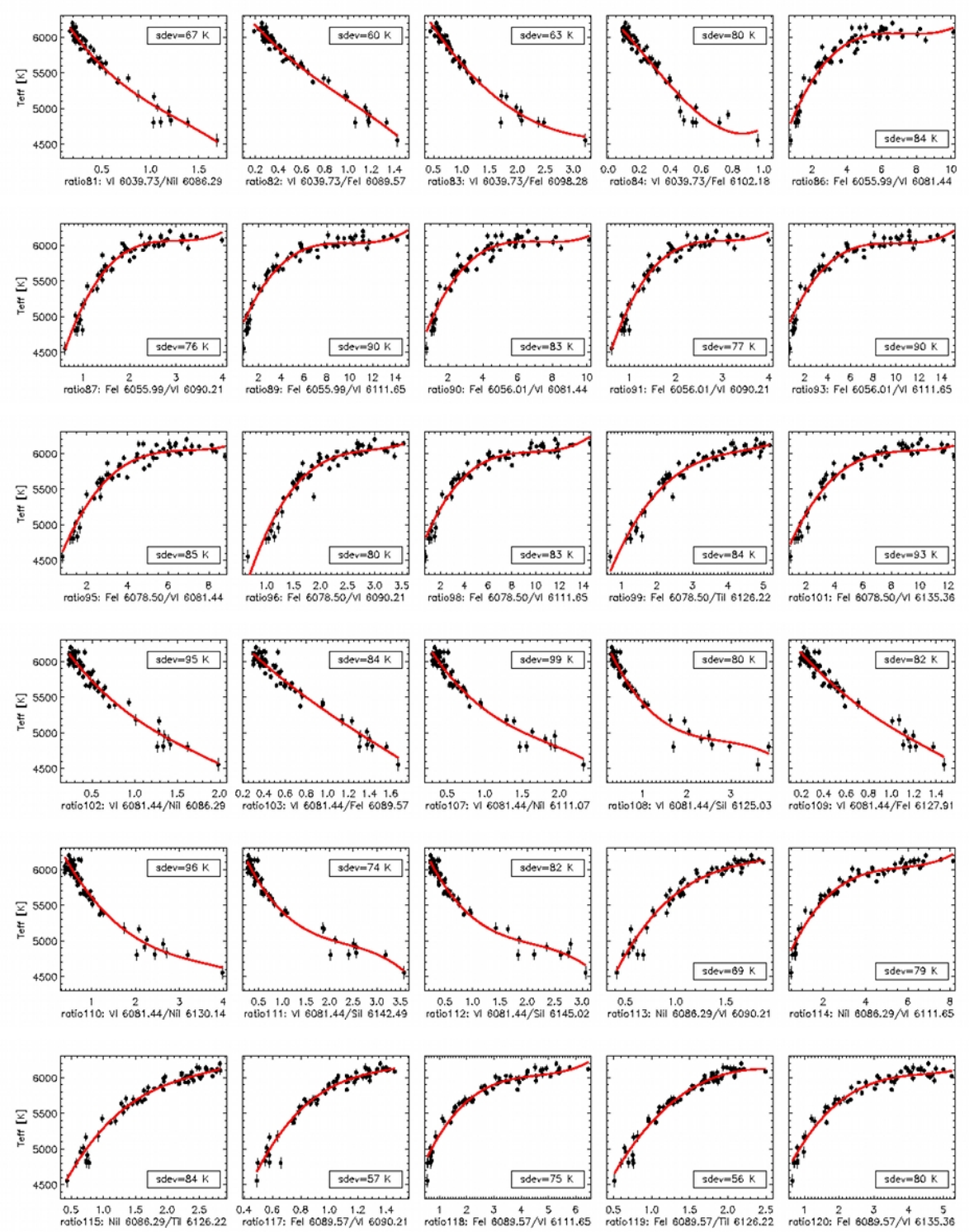
Teff [K]
sdev=67 K
ratio81: VI 6039.73/NiI 6086.29
sdev=60 K
ratio82: VI 6039.73/FeI 6089.57
sdev=63 K
ratio83: VI 6039.73/FeI 6098.28
sdev=80 K
ratio84: VI 6039.73/FeI 6102.18
sdev=84 K
ratio86: FeI 6055.99/VI 6081.44
sdev=76 K
ratio87: FeI 6055.99/VI 6090.21
sdev=90 K
ratio89: FeI 6055.99/VI 6111.65
sdev=83 K
ratio90: FeI 6056.01/VI 6081.44
sdev=77 K
ratio91: FeI 6056.01/VI 6090.21
sdev=90 K
ratio93: FeI 6056.01/VI 6111.65
sdev=85 K
ratio95: FeI 6078.50/VI 6081.44
sdev=80 K
ratio96: FeI 6078.50/VI 6090.21
sdev=83 K
ratio98: FeI 6078.50/VI 6111.65
sdev=84 K
ratio99: FeI 6078.50/TiI 6126.22
sdev=93 K
ratio101: FeI 6078.50/VI 6135.36
sdev=95 K
ratio102: VI 6081.44/NiI 6086.29
sdev=84 K
ratio103: VI 6081.44/FeI 6089.57
sdev=99 K
ratio107: VI 6081.44/NiI 6111.07
sdev=80 K
ratio108: VI 6081.44/SiI 6125.03
sdev=82 K
ratio109: VI 6081.44/FeI 6127.91
sdev=96 K
ratio110: VI 6081.44/NiI 6130.14
sdev=74 K
ratio111: VI 6081.44/SiI 6142.49
sdev=82 K
ratio112: VI 6081.44/SiI 6145.02
sdev=69 K
ratio113: NiI 6086.29/VI 6090.21
sdev=79 K
ratio114: NiI 6086.29/VI 6111.65
sdev=84 K
ratio115: NiI 6086.29/TiI 6126.22
sdev=57 K
ratio117: FeI 6089.57/VI 6090.21
sdev=75 K
ratio118: FeI 6089.57/VI 6111.65
sdev=56 K
ratio119: FeI 6089.57/TiI 6126.22
sdev=80 K
ratio120: FeI 6089.57/VI 6135.36

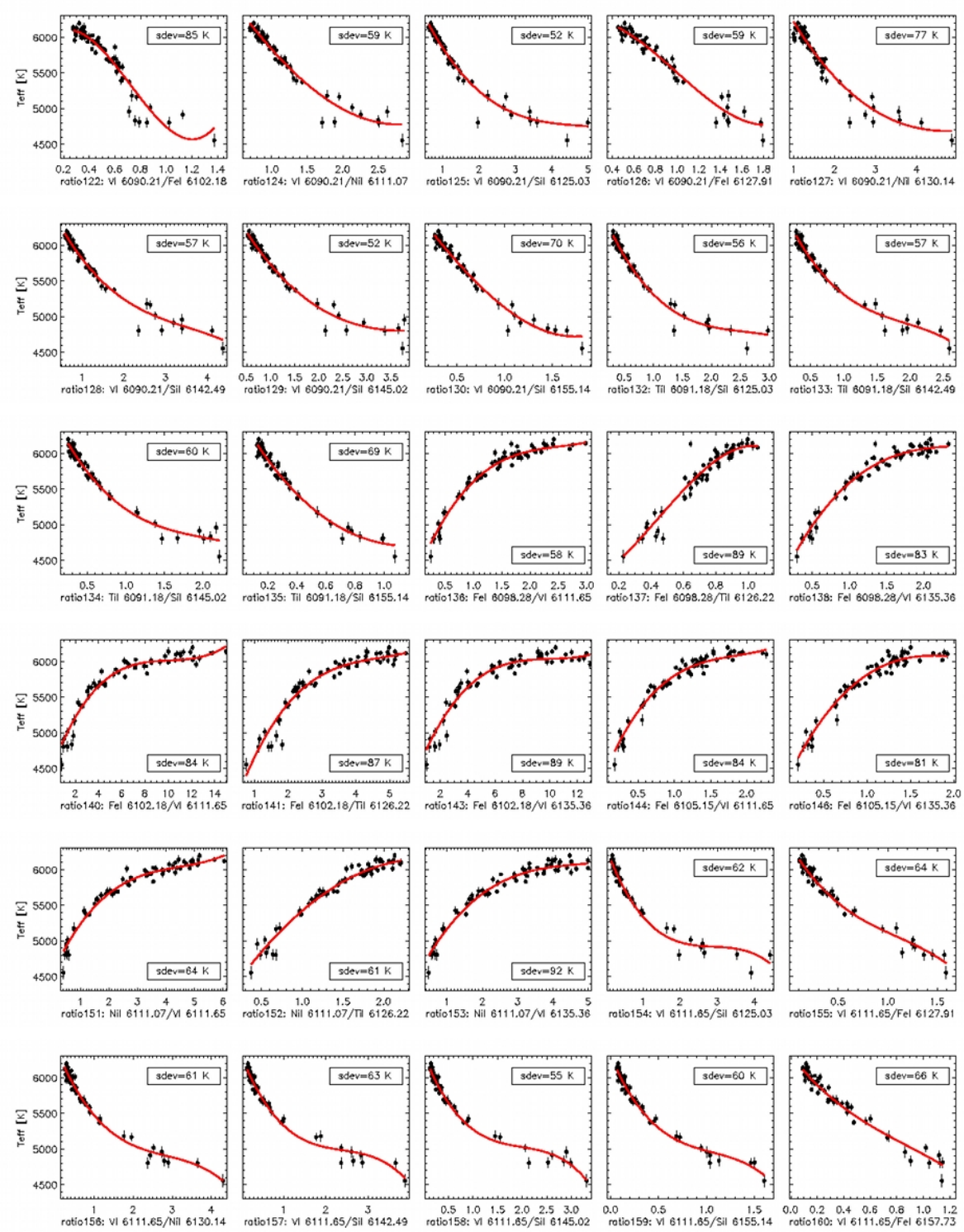
Teff [K]
sdev=85 K
ratio122: VI 6090.21/FeI 6102.18
sdev=59 K
ratio124: VI 6090.21/NiI 6111.07
sdev=52 K
ratio125: VI 6090.21/SiI 6125.03
sdev=59 K
ratio126: VI 6090.21/FeI 6127.91
sdev=77 K
ratio127: VI 6090.21/NiI 6130.14
sdev=57 K
ratio128: VI 6090.21/SiI 6142.49
sdev=52 K
ratio129: VI 6090.21/SiI 6145.02
sdev=70 K
ratio130: VI 6090.21/SiI 6155.14
sdev=56 K
ratio132: TiI 6091.18/SiI 6125.03
sdev=57 K
ratio133: TiI 6091.18/SiI 6142.49
sdev=60 K
ratio134: TiI 6091.18/SiI 6145.02
sdev=69 K
ratio135: TiI 6091.18/SiI 6155.14
sdev=58 K
ratio136: FeI 6098.28/VI 6111.65
sdev=89 K
ratio137: FeI 6098.28/TiI 6126.22
sdev=83 K
ratio138: FeI 6098.28/VI 6135.36
sdev=84 K
ratio140: FeI 6102.18/VI 6111.65
sdev=87 K
ratio141: FeI 6102.18/TiI 6126.22
sdev=89 K
ratio143: FeI 6102.18/VI 6135.36
sdev=84 K
ratio144: FeI 6105.15/VI 6111.65
sdev=81 K
ratio146: FeI 6105.15/VI 6135.36
sdev=64 K
ratio151: NiI 6111.07/VI 6111.65
sdev=61 K
ratio152: NiI 6111.07/TiI 6126.22
sdev=92 K
ratio153: NiI 6111.07/VI 6135.36
sdev=62 K
ratio154: VI 6111.65/SiI 6125.03
sdev=64 K
ratio155: VI 6111.65/FeI 6127.91
sdev=61 K
ratio156: VI 6111.65/NiI 6130.14
sdev=63 K
ratio157: VI 6111.65/SiI 6142.49
sdev=55 K
ratio158: VI 6111.65/SiI 6145.02
sdev=60 K
ratio159: VI 6111.65/SiI 6155.14
sdev=66 K
ratio160: VI 6111.65/FeI 6157.73

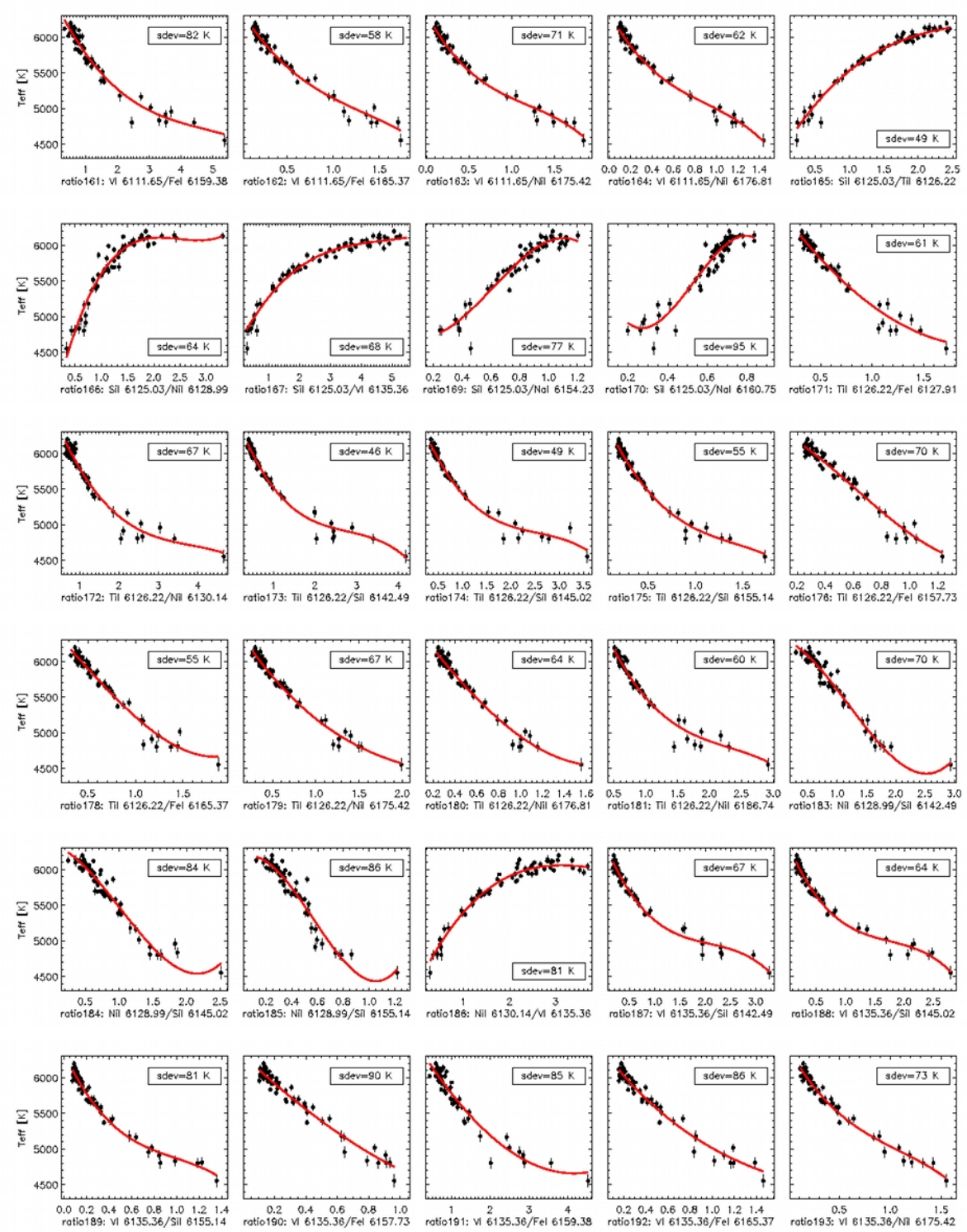
Teff [K]
sdev=82 K
ratio161: VI 6111.65/FeI 6159.38
sdev=58 K
ratio162: VI 6111.65/FeI 6165.37
sdev=71 K
ratio163: VI 6111.65/NiI 6175.42
sdev=62 K
ratio164: VI 6111.65/NiI 6176.81
sdev=49 K
ratio165: SiI 6125.03/TiI 6126.22
sdev=64 K
ratio166: SiI 6125.03/NiI 6128.99
sdev=68 K
ratio167: SiI 6125.03/VI 6135.36
sdev=77 K
ratio169: SiI 6125.03/NaI 6154.23
sdev=95 K
ratio170: SiI 6125.03/NaI 6160.75
sdev=61 K
ratio171: TiI 6126.22/FeI 6127.91
sdev=67 K
ratio172: TiI 6126.22/NiI 6130.14
sdev=46 K
ratio173: TiI 6126.22/SiI 6142.49
sdev=49 K
ratio174: TiI 6126.22/SiI 6145.02
sdev=55 K
ratio175: TiI 6126.22/SiI 6155.14
sdev=70 K
ratio176: TiI 6126.22/FeI 6157.73
sdev=55 K
ratio178: TiI 6126.22/FeI 6165.37
sdev=67 K
ratio179: TiI 6126.22/NiI 6175.42
sdev=64 K
ratio180: TiI 6126.22/NiI 6176.81
sdev=60 K
ratio181: TiI 6126.22/NiI 6186.74
sdev=70 K
ratio183: NiI 6128.99/SiI 6142.49
sdev=84 K
ratio184: NiI 6128.99/SiI 6145.02
sdev=86 K
ratio185: NiI 6128.99/SiI 6155.14
sdev=81 K
ratio186: NiI 6130.14/VI 6135.36
sdev=67 K
ratio187: VI 6135.36/SiI 6142.49
sdev=64 K
ratio188: VI 6135.36/SiI 6145.02
sdev=81 K
ratio189: VI 6135.36/SiI 6155.14
sdev=90 K
ratio190: VI 6135.36/FeI 6157.73
sdev=85 K
ratio191: VI 6135.36/FeI 6159.38
sdev=86 K
ratio192: VI 6135.36/FeI 6165.37
sdev=73 K
ratio193: VI 6135.36/NiI 6175.42

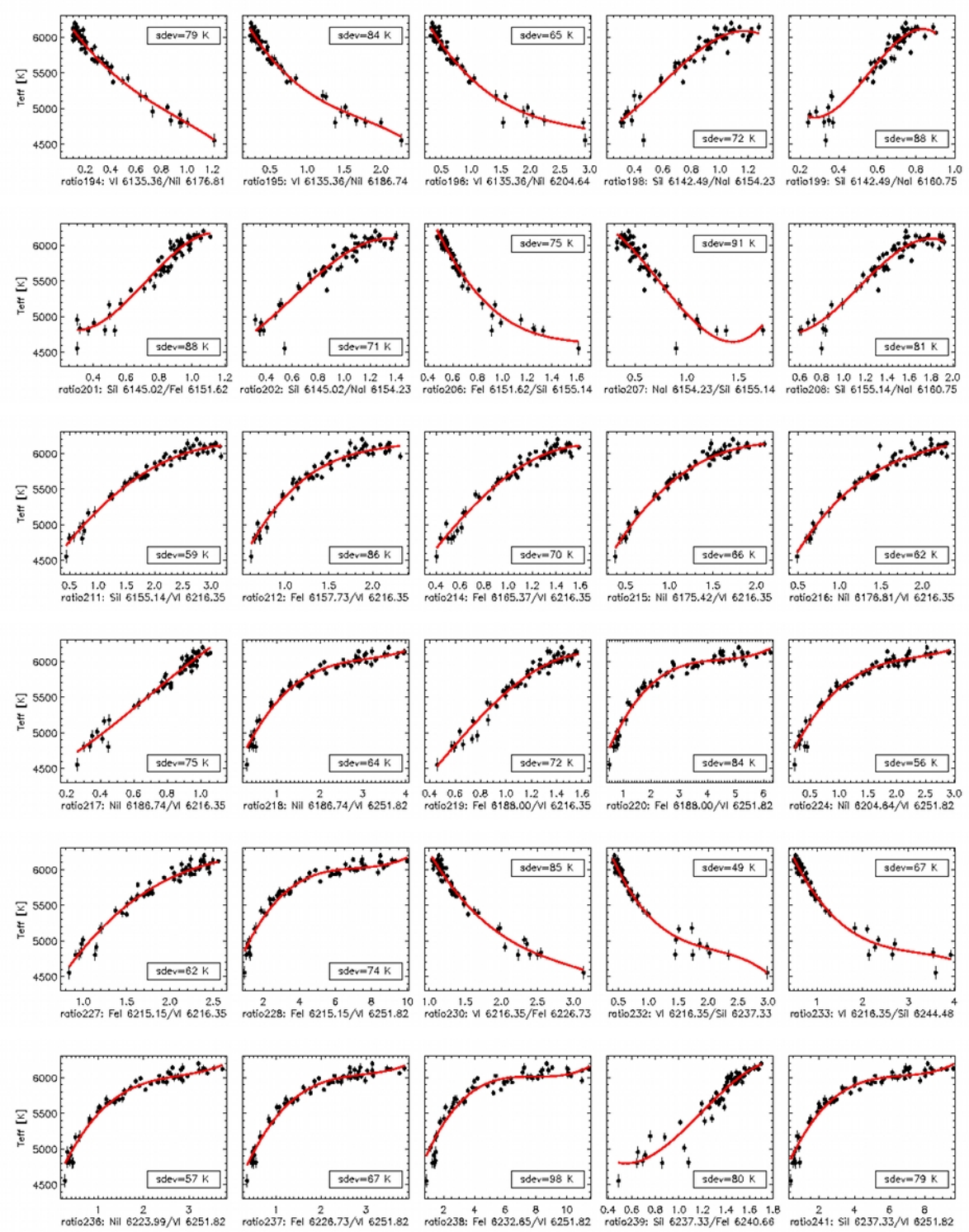
Teff [K]
sdev=79 K
ratio194: VI 6135.36/NII 6176.81
sdev=84 K
ratio195: VI 6135.36/NII 6186.74
sdev=65 K
ratio196: VI 6135.36/NII 6204.64
sdev=72 K
ratio198: SII 6142.49/NaI 6154.23
sdev=88 K
ratio199: SII 6142.49/NaI 6160.75
sdev=88 K
ratio201: SII 6145.02/FeI 6151.62
sdev=71 K
ratio202: SII 6145.02/NaI 6154.23
sdev=75 K
ratio206: FeI 6151.62/SII 6155.14
sdev=91 K
ratio207: NaI 6154.23/SII 6155.14
sdev=81 K
ratio208: SII 6155.14/NaI 6160.75
sdev=59 K
ratio211: SII 6155.14/VI 6216.35
sdev=86 K
ratio212: FeI 6157.73/VI 6216.35
sdev=70 K
ratio214: FeI 6165.37/VI 6216.35
sdev=66 K
ratio215: NII 6175.42/VI 6216.35
sdev=62 K
ratio216: NII 6176.81/VI 6216.35
sdev=75 K
ratio217: NII 6186.74/VI 6216.35
sdev=64 K
ratio218: NII 6186.74/VI 6251.82
sdev=72 K
ratio219: FeI 6188.00/VI 6216.35
sdev=84 K
ratio220: FeI 6188.00/VI 6251.82
sdev=56 K
ratio224: NII 6204.64/VI 6251.82
sdev=62 K
ratio227: FeI 6215.15/VI 6216.35
sdev=74 K
ratio228: FeI 6215.15/VI 6251.82
sdev=85 K
ratio230: VI 6216.35/FeI 6226.73
sdev=49 K
ratio232: VI 6216.35/SII 6237.33
sdev=67 K
ratio233: VI 6216.35/SII 6244.48
sdev=57 K
ratio236: NII 6223.99/VI 6251.82
sdev=67 K
ratio237: FeI 6226.73/VI 6251.82
sdev=98 K
ratio238: FeI 6232.65/VI 6251.82
sdev=80 K
ratio239: SII 6237.33/FeI 6240.66
sdev=79 K
ratio241: SII 6237.33/VI 6251.82

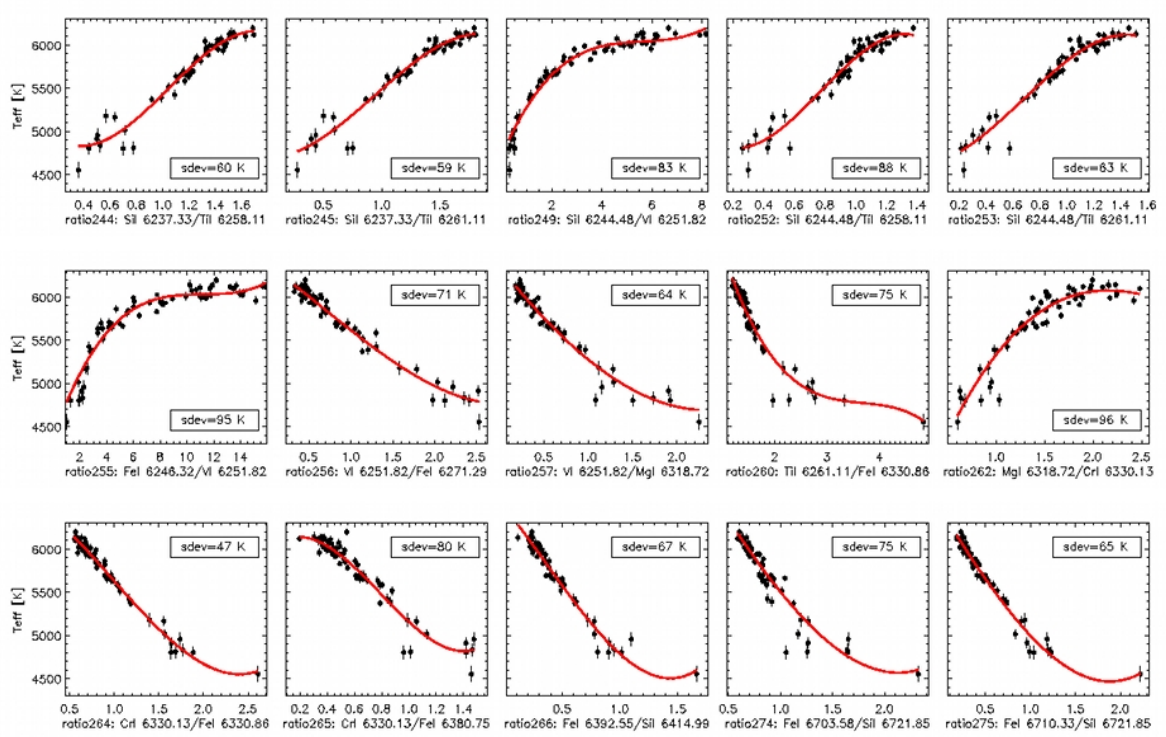
Teff [K]
sdev=60 K
ratio244: SiI 6237.33/TiI 6258.11
sdev=59 K
ratio245: SiI 6237.33/TiI 6261.11
sdev=83 K
ratio249: SiI 6244.48/VI 6251.82
sdev=88 K
ratio252: SiI 6244.48/TiI 6258.11
sdev=83 K
ratio253: SiI 6244.48/TiI 6261.11
sdev=95 K
ratio255: FeI 6246.32/VI 6251.82
sdev=71 K
ratio256: VI 6251.82/FeI 6271.29
sdev=64 K
ratio257: VI 6251.82/MgI 6318.72
sdev=75 K
ratio260: TiI 6261.11/FeI 6330.86
sdev=96 K
ratio262: MgI 6318.72/CrI 6330.13
sdev=47 K
ratio264: CrI 6330.13/FeI 6330.86
sdev=80 K
ratio265: CrI 6330.13/FeI 6380.75
sdev=67 K
ratio266: FeI 6392.55/SiI 6414.99
sdev=75 K
ratio274: FeI 6703.58/SiI 6721.85
sdev=65 K
ratio275: FeI 6710.33/SiI 6721.85

### 5.5.4 List of the line ratios and their calibration coefficients

Table 5.6: List of the 190 equivalent width ratios ($rEW_k$) calibrated against temperature ($T_{\rm eff}$) as $3^{rd}$ order polynomial functions. The polynomial function is $T^k_{eff} = c_0 + c_1 * rEW_k + c_2 * rEW_k^2 + c_3 * rEW_k^3$ with $c_0$, $c_1$, $c_2$ and $c_3$ the coefficients of the $2^{nd}$ order polynomial function. "ratio" is the ratio identification number given in this study. "std" is the standard deviation (1.48*MAD) of the points around the polynomial fit (printed as "sdev" in Figure 5.5).

| ratio | std | line 1 | line 2 | $c_0$ | $c_1$ | $c_2$ | $c_3$ |
|---|---|---|---|---|---|---|---|
| 0 | 71 | TiI 5490.15 | SiI 5517.53 | 6651.07 | -586.95 | 13.40 | 6.15 |
| 8 | 72 | FeI 5619.60 | VI 5670.85 | 3719.77 | 2565.28 | -1008.76 | 142.20 |
| 9 | 62 | SiI 5621.60 | VI 5670.85 | 4437.02 | 3985.89 | -3032.56 | 708.43 |
| 10 | 66 | FeI 5633.97 | VI 5670.85 | 4090.92 | 1262.39 | -286.55 | 22.09 |
| 11 | 70 | FeI 5633.97 | VI 5703.59 | 2957.03 | 3479.63 | -1349.64 | 177.58 |
| 12 | 65 | FeI 5650.71 | VI 5670.85 | 4151.17 | 1848.12 | -653.23 | 81.52 |
| 13 | 91 | FeI 5650.71 | VI 5703.59 | 3495.73 | 3983.64 | -2170.97 | 418.24 |
| 14 | 43 | FeI 5651.47 | VI 5670.85 | 3743.38 | 4476.96 | -3096.91 | 774.50 |
| 15 | 79 | FeI 5651.47 | VI 5703.59 | 2964.10 | 7837.76 | -4851.15 | -94.44 |
| 16 | 83 | FeI 5662.52 | VI 5670.85 | 3902.30 | 1017.41 | -166.92 | 9.20 |
| 17 | 93 | FeI 5662.52 | VI 5703.59 | 2337.74 | 3095.76 | -875.30 | 82.88 |
| 18 | 91 | FeI 5662.52 | VI 5727.05 | 2313.54 | 3701.09 | -1256.53 | 144.21 |
| 19 | 79 | VI 5670.85 | FeI 5680.26 | 6509.60 | -154.64 | -169.33 | 26.25 |
| 20 | 73 | VI 5670.85 | NiI 5682.20 | 6367.58 | -1351.32 | 318.97 | -22.80 |
| 21 | 80 | VI 5670.85 | SiI 5690.43 | 6359.31 | -1327.39 | 386.69 | -50.97 |
| 22 | 66 | VI 5670.85 | SiI 5701.11 | 6356.71 | -1029.41 | 160.05 | 0.90 |
| 23 | 77 | VI 5670.85 | FeI 5705.99 | 6282.13 | -1580.51 | -1211.63 | 1217.36 |
| 24 | 79 | VI 5670.85 | MgI 5711.09 | 6123.64 | 10.83 | -6115.10 | 4657.15 |
| 25 | 97 | VI 5670.85 | FeI 5717.85 | 6368.22 | -1524.61 | -140.82 | 261.48 |
| 26 | 71 | VI 5670.85 | FeI 5731.77 | 6293.14 | -1006.38 | -296.36 | 153.82 |
| 30 | 68 | NiI 5682.20 | VI 5703.59 | 3327.65 | 3672.50 | -1763.17 | 298.53 |
| 31 | 54 | NiI 5682.20 | VI 5727.05 | 3611.60 | 3580.20 | -1871.07 | 351.96 |
| 32 | 78 | NiI 5682.20 | VI 5737.07 | 4390.77 | 811.85 | -142.30 | 8.46 |
| 34 | 60 | SiI 5690.43 | VI 5703.59 | 3722.71 | 2957.22 | -1304.30 | 200.26 |
| 35 | 49 | SiI 5690.43 | VI 5727.05 | 3793.06 | 3373.91 | -1804.31 | 347.64 |
| 36 | 85 | SiI 5690.43 | VI 5737.07 | 4461.86 | 787.29 | -140.96 | 8.60 |
| 37 | 53 | SiI 5701.11 | VI 5703.59 | 3566.43 | 4023.01 | -2314.45 | 473.85 |
| 38 | 47 | SiI 5701.11 | VI 5727.05 | 3733.14 | 4225.35 | -2760.41 | 656.32 |
| 39 | 75 | SiI 5701.11 | VI 5737.07 | 4424.06 | 995.87 | -219.87 | 16.55 |
| 41 | 87 | VI 5703.59 | FeI 5705.99 | 6152.58 | 549.08 | -4380.79 | 2413.51 |
| 44 | 74 | VI 5703.59 | FeI 5731.77 | 6035.30 | 663.39 | -1671.33 | 367.88 |
| 45 | 73 | VI 5703.59 | FeI 5753.12 | 5884.85 | 1692.04 | -4416.16 | 1764.89 |
| 46 | 67 | VI 5703.59 | SiI 5753.65 | 6409.02 | -522.77 | -537.28 | 195.41 |
| 47 | 89 | VI 5703.59 | SiI 5772.15 | 6460.62 | -1085.55 | 179.41 | -1.22 |
| 48 | 75 | FeI 5705.99 | VI 5727.05 | 3822.58 | 1629.31 | -400.31 | 33.82 |
| 49 | 86 | FeI 5705.99 | VI 5737.07 | 4390.87 | 440.72 | -41.68 | 1.33 |
| 50 | 90 | MgI 5711.09 | VI 5727.05 | 1750.73 | 3865.29 | -1184.85 | 122.32 |
| 54 | 65 | VI 5727.05 | FeI 5731.77 | 6151.00 | 336.93 | -1207.43 | 313.34 |
| 55 | 65 | VI 5727.05 | FeI 5753.12 | 6021.76 | 898.15 | -2639.55 | 949.23 |
| 56 | 64 | VI 5727.05 | SiI 5753.65 | 6619.42 | -993.22 | 11.97 | 37.94 |
| 57 | 88 | VI 5727.05 | SiI 5772.15 | 6493.94 | -1000.77 | 171.07 | -6.78 |
| 58 | 91 | FeI 5731.77 | VI 5737.07 | 4187.47 | 874.82 | -144.46 | 7.99 |
| 59 | 89 | VI 5737.07 | FeI 5753.12 | 6205.50 | -1809.29 | -621.43 | 929.32 |
| 60 | 75 | VI 5737.07 | SiI 5753.65 | 6302.65 | -1900.57 | 813.35 | -129.06 |

| ratio | std | line 1 | line 2 | $c_0$ | $c_1$ | $c_2$ | $c_3$ |
|---|---|---|---|---|---|---|---|
| 64 | 63 | FeI 5852.23 | TiI 5866.45 | 2862.44 | 1680.16 | 5380.29 | -3835.08 |
| 66 | 53 | FeI 5856.09 | TiI 5866.45 | 5667.04 | -8307.49 | 20059.59 | -11372.40 |
| 67 | 94 | FeI 5862.36 | TiI 5866.45 | 3128.31 | 2843.11 | -883.86 | 90.41 |
| 68 | 66 | SiI 5948.55 | FeI 5956.70 | 3158.16 | 2110.05 | -153.28 | -88.88 |
| 69 | 92 | SiI 5948.55 | NiI 6007.31 | 2017.67 | 2509.53 | -517.22 | 35.51 |
| 70 | 88 | FeI 5983.69 | VI 6039.73 | 4171.05 | 764.58 | -108.24 | 5.23 |
| 72 | 89 | FeI 5987.05 | VI 6039.73 | 4093.37 | 753.59 | -102.35 | 4.83 |
| 75 | 86 | FeI 6007.96 | VI 6039.73 | 4213.30 | 801.07 | -122.41 | 6.50 |
| 78 | 65 | VI 6039.73 | FeI 6055.99 | 6312.44 | -2149.28 | 145.51 | 323.98 |
| 79 | 65 | VI 6039.73 | FeI 6056.01 | 6311.11 | -2133.79 | 99.70 | 353.27 |
| 80 | 70 | VI 6039.73 | FeI 6078.50 | 6328.51 | -2287.81 | -864.99 | 1350.92 |
| 81 | 67 | VI 6039.73 | NiI 6086.29 | 6485.36 | -2301.72 | 1193.10 | -304.55 |
| 82 | 60 | VI 6039.73 | FeI 6089.57 | 6561.61 | -2185.47 | 1107.17 | -372.24 |
| 83 | 63 | VI 6039.73 | FeI 6098.28 | 6789.35 | -1429.67 | 287.16 | -16.71 |
| 84 | 80 | VI 6039.73 | FeI 6102.18 | 6320.05 | -2217.56 | -1597.46 | 2228.72 |
| 86 | 84 | FeI 6055.99 | VI 6081.44 | 4293.63 | 735.90 | -101.59 | 4.63 |
| 87 | 76 | FeI 6055.99 | VI 6090.21 | 3074.97 | 2943.33 | -971.68 | 107.61 |
| 89 | 90 | FeI 6055.99 | VI 6111.65 | 4657.40 | 410.46 | -40.89 | 1.36 |
| 90 | 83 | FeI 6056.01 | VI 6081.44 | 4291.53 | 737.11 | -101.80 | 4.64 |
| 91 | 77 | FeI 6056.01 | VI 6090.21 | 3066.86 | 2953.01 | -975.36 | 108.06 |
| 93 | 90 | FeI 6056.01 | VI 6111.65 | 4656.65 | 410.77 | -40.93 | 1.36 |
| 95 | 85 | FeI 6078.50 | VI 6081.44 | 4010.17 | 849.49 | -119.80 | 5.71 |
| 96 | 80 | FeI 6078.50 | VI 6090.21 | 2328.04 | 3628.28 | -1207.11 | 137.32 |
| 98 | 83 | FeI 6078.50 | VI 6111.65 | 4518.26 | 442.06 | -44.25 | 1.51 |
| 99 | 84 | FeI 6078.50 | TiI 6126.22 | 3389.50 | 1618.83 | -346.54 | 26.25 |
| 101 | 93 | FeI 6078.50 | VI 6135.36 | 4306.61 | 527.26 | -54.36 | 1.90 |
| 102 | 95 | VI 6081.44 | NiI 6086.29 | 6503.44 | -1860.41 | 693.46 | -124.54 |
| 103 | 84 | VI 6081.44 | FeI 6089.57 | 6537.99 | -1567.43 | 399.57 | -82.37 |
| 107 | 99 | VI 6081.44 | NiI 6111.07 | 6667.95 | -2049.50 | 861.20 | -153.21 |
| 108 | 80 | VI 6081.44 | SiI 6125.03 | 6504.55 | -1549.44 | 520.84 | -62.19 |
| 109 | 82 | VI 6081.44 | FeI 6127.91 | 6497.62 | -2072.23 | 844.96 | -193.58 |
| 110 | 96 | VI 6081.44 | NiI 6130.14 | 6641.71 | -1322.00 | 320.60 | -29.08 |
| 111 | 74 | VI 6081.44 | SiI 6142.49 | 6482.59 | -1590.74 | 599.55 | -84.96 |
| 112 | 82 | VI 6081.44 | SiI 6145.02 | 6490.29 | -1805.29 | 768.02 | -122.15 |
| 113 | 69 | NiI 6086.29 | VI 6090.21 | 3181.81 | 4216.20 | -2122.91 | 380.77 |
| 114 | 79 | NiI 6086.29 | VI 6111.65 | 4555.56 | 717.86 | -121.52 | 7.18 |
| 115 | 84 | NiI 6086.29 | TiI 6126.22 | 3767.75 | 2165.20 | -732.89 | 92.56 |
| 117 | 57 | FeI 6089.57 | VI 6090.21 | 1796.06 | 8272.26 | -5482.17 | 1266.13 |
| 118 | 75 | FeI 6089.57 | VI 6111.65 | 4412.66 | 973.78 | -203.52 | 14.87 |
| 119 | 56 | FeI 6089.57 | TiI 6126.22 | 3546.35 | 2566.59 | -816.51 | 80.89 |
| 120 | 80 | FeI 6089.57 | VI 6135.36 | 4160.82 | 1181.74 | -254.48 | 18.97 |
| 122 | 85 | VI 6090.21 | FeI 6102.18 | 5782.13 | 2907.25 | -7343.66 | 3398.69 |
| 124 | 59 | VI 6090.21 | NiI 6111.07 | 7194.51 | -1580.02 | 198.05 | 20.70 |
| 125 | 52 | VI 6090.21 | SiI 6125.03 | 6850.89 | -1231.87 | 248.36 | -17.19 |
| 126 | 59 | VI 6090.21 | FeI 6127.91 | 6207.53 | 594.07 | -1952.97 | 655.31 |
| 127 | 77 | VI 6090.21 | NiI 6130.14 | 7337.94 | -1310.85 | 198.56 | -8.45 |
| 128 | 57 | VI 6090.21 | SiI 6142.49 | 6828.16 | -1301.18 | 313.41 | -29.40 |
| 129 | 52 | VI 6090.21 | SiI 6145.02 | 6768.10 | -1295.37 | 273.41 | -18.09 |
| 130 | 70 | VI 6090.21 | SiI 6155.14 | 6588.87 | -1754.46 | 157.93 | 134.53 |
| 132 | 56 | TiI 6091.18 | SiI 6125.03 | 6690.51 | -2039.99 | 760.01 | -98.89 |
| 133 | 57 | TiI 6091.18 | SiI 6142.49 | 6680.19 | -2184.20 | 986.58 | -171.45 |
| 134 | 60 | TiI 6091.18 | SiI 6145.02 | 6647.95 | -2278.64 | 1012.81 | -164.87 |
| 135 | 69 | TiI 6091.18 | SiI 6155.14 | 6536.00 | -3535.05 | 2050.48 | -317.21 |
| 136 | 58 | FeI 6098.28 | VI 6111.65 | 4305.49 | 1929.15 | -722.75 | 95.13 |
| 137 | 89 | FeI 6098.28 | TiI 6126.22 | 4165.96 | 1105.33 | 3324.08 | -2493.09 |
| 138 | 83 | FeI 6098.28 | VI 6135.36 | 4047.30 | 2284.61 | -848.08 | 105.20 |
| 140 | 84 | FeI 6102.18 | VI 6111.65 | 4510.74 | 432.30 | -42.08 | 1.39 |

| ratio | std | line 1 | line 2 | $c_0$ | $c_1$ | $c_2$ | $c_3$ |
|---|---|---|---|---|---|---|---|
| 141 | 87 | FeI 6102.18 | TiI 6126.22 | 3401.96 | 1537.51 | -310.82 | 22.06 |
| 143 | 89 | FeI 6102.18 | VI 6135.36 | 4318.85 | 502.50 | -49.56 | 1.65 |
| 144 | 84 | FeI 6105.15 | VI 6111.65 | 4344.02 | 2480.20 | -1246.48 | 223.82 |
| 146 | 81 | FeI 6105.15 | VI 6135.36 | 4142.15 | 2703.59 | -1190.02 | 159.38 |
| 151 | 64 | NiI 6111.07 | VI 6111.65 | 4532.10 | 872.62 | -179.73 | 13.41 |
| 152 | 61 | NiI 6111.07 | TiI 6126.22 | 4097.05 | 1678.04 | -358.40 | 6.53 |
| 153 | 92 | NiI 6111.07 | VI 6135.36 | 4370.54 | 982.79 | -195.78 | 13.58 |
| 154 | 62 | VI 6111.65 | SiI 6125.03 | 6311.94 | -1391.68 | 471.78 | -54.33 |
| 155 | 64 | VI 6111.65 | FeI 6127.91 | 6371.37 | -2358.61 | 1592.89 | -487.47 |
| 156 | 61 | VI 6111.65 | NiI 6130.14 | 6444.33 | -1347.38 | 424.69 | -49.66 |
| 157 | 63 | VI 6111.65 | SiI 6142.49 | 6309.60 | -1480.01 | 580.14 | -80.78 |
| 158 | 55 | VI 6111.65 | SiI 6145.02 | 6320.53 | -1718.80 | 806.34 | -135.22 |
| 159 | 60 | VI 6111.65 | SiI 6155.14 | 6295.15 | -3084.65 | 2571.62 | -807.15 |
| 160 | 66 | VI 6111.65 | FeI 6157.73 | 6316.00 | -2377.82 | 1579.68 | -592.26 |
| 161 | 82 | VI 6111.65 | FeI 6159.38 | 6531.14 | -923.32 | 170.58 | -11.98 |
| 162 | 58 | VI 6111.65 | FeI 6165.37 | 6367.28 | -2041.60 | 1088.46 | -270.55 |
| 163 | 71 | VI 6111.65 | NiI 6175.42 | 6334.45 | -2229.90 | 1446.35 | -405.24 |
| 164 | 62 | VI 6111.65 | NiI 6176.81 | 6337.87 | -2741.73 | 2217.93 | -821.53 |
| 165 | 49 | SiI 6125.03 | TiI 6126.22 | 4366.21 | 1611.03 | -502.22 | 56.72 |
| 166 | 64 | SiI 6125.03 | NiI 6128.99 | 3452.30 | 3338.67 | -1374.99 | 184.53 |
| 167 | 68 | SiI 6125.03 | VI 6135.36 | 4597.15 | 832.19 | -165.35 | 11.65 |
| 169 | 77 | SiI 6125.03 | NaI 6154.23 | 4789.24 | -1204.61 | 5412.64 | -2938.84 |
| 170 | 95 | SiI 6125.03 | NaI 6160.75 | 6213.43 | -11523.86 | 28659.88 | -17971.25 |
| 171 | 61 | TiI 6126.22 | FeI 6127.91 | 6716.18 | -2062.53 | 501.65 | -1.37 |
| 172 | 67 | TiI 6126.22 | NiI 6130.14 | 7058.67 | -1625.93 | 396.46 | -34.47 |
| 173 | 46 | TiI 6126.22 | SiI 6142.49 | 6690.16 | -1652.12 | 544.13 | -65.01 |
| 174 | 49 | TiI 6126.22 | SiI 6145.02 | 6683.80 | -1822.27 | 656.93 | -85.87 |
| 175 | 55 | TiI 6126.22 | SiI 6155.14 | 6605.17 | -3093.99 | 1869.77 | -436.02 |
| 176 | 70 | TiI 6126.22 | FeI 6157.73 | 6398.68 | -905.13 | -1348.64 | 732.82 |
| 178 | 55 | TiI 6126.22 | FeI 6165.37 | 6630.51 | -1405.85 | -219.90 | 219.33 |
| 179 | 67 | TiI 6126.22 | NiI 6175.42 | 6634.37 | -1967.49 | 594.97 | -63.72 |
| 180 | 64 | TiI 6126.22 | NiI 6176.81 | 6585.46 | -2080.90 | 337.35 | 105.37 |
| 181 | 60 | TiI 6126.22 | NiI 6186.74 | 7263.94 | -2645.08 | 1021.40 | -147.03 |
| 183 | 70 | NiI 6128.99 | SiI 6142.49 | 6338.91 | -198.62 | -744.87 | 207.42 |
| 184 | 84 | NiI 6128.99 | SiI 6145.02 | 6354.53 | -253.29 | -933.85 | 306.67 |
| 185 | 86 | NiI 6128.99 | SiI 6155.14 | 6155.73 | 912.59 | -6390.65 | 3771.88 |
| 186 | 81 | NiI 6130.14 | VI 6135.36 | 4379.06 | 1337.90 | -339.65 | 26.76 |
| 187 | 67 | VI 6135.36 | SiI 6142.49 | 6383.84 | -1731.06 | 755.16 | -121.13 |
| 188 | 64 | VI 6135.36 | SiI 6145.02 | 6389.86 | -1974.28 | 1008.34 | -191.61 |
| 189 | 81 | VI 6135.36 | SiI 6155.14 | 6348.89 | -3419.76 | 2923.22 | -985.49 |
| 190 | 90 | VI 6135.36 | FeI 6157.73 | 6314.54 | -2063.00 | 391.82 | 65.27 |
| 191 | 85 | VI 6135.36 | FeI 6159.38 | 6570.02 | -887.59 | 95.11 | 1.87 |
| 192 | 86 | VI 6135.36 | FeI 6165.37 | 6402.93 | -2028.32 | 751.95 | -115.22 |
| 193 | 73 | VI 6135.36 | NiI 6175.42 | 6404.91 | -2528.13 | 1675.67 | -515.87 |
| 194 | 79 | VI 6135.36 | NiI 6176.81 | 6371.88 | -2771.62 | 1857.47 | -660.58 |
| 195 | 84 | VI 6135.36 | NiI 6186.74 | 6547.48 | -2077.52 | 951.92 | -182.12 |
| 196 | 65 | VI 6135.36 | NiI 6204.64 | 6592.69 | -1607.78 | 494.39 | -55.91 |
| 198 | 72 | SiI 6142.49 | NaI 6154.23 | 4592.53 | -44.37 | 3339.47 | -1887.20 |
| 199 | 88 | SiI 6142.49 | NaI 6160.75 | 6074.37 | -9786.17 | 23624.87 | -14186.05 |
| 201 | 88 | SiI 6145.02 | FeI 6151.62 | 5481.57 | -4850.00 | 10136.05 | -4691.07 |
| 202 | 71 | SiI 6145.02 | NaI 6154.23 | 4480.67 | 505.59 | 1954.58 | -1068.74 |
| 206 | 75 | FeI 6151.62 | SiI 6155.14 | 8627.01 | -6789.43 | 3944.25 | -783.23 |
| 207 | 91 | NaI 6154.23 | SiI 6155.14 | 6379.82 | 23.60 | -2530.62 | 1165.35 |
| 208 | 81 | SiI 6155.14 | NaI 6160.75 | 5505.77 | -3285.43 | 4201.39 | -1218.84 |
| 211 | 59 | SiI 6155.14 | VI 6216.35 | 4240.13 | 1152.70 | -192.73 | 4.73 |
| 212 | 86 | FeI 6157.73 | VI 6216.35 | 2929.13 | 3820.32 | -1589.74 | 230.07 |
| 214 | 70 | FeI 6165.37 | VI 6216.35 | 3741.62 | 2492.09 | -397.55 | -147.42 |

| ratio | std | line 1 | line 2 | $c_0$ | $c_1$ | $c_2$ | $c_3$ |
|---|---|---|---|---|---|---|---|
| 215 | 66 | NiI 6175.42 | VI 6216.35 | 3825.95 | 2560.29 | -920.34 | 107.02 |
| 216 | 62 | NiI 6176.81 | VI 6216.35 | 3500.33 | 2739.20 | -1020.57 | 140.44 |
| 217 | 75 | NiI 6186.74 | VI 6216.35 | 4386.23 | 1024.44 | 1356.25 | -668.51 |
| 218 | 64 | NiI 6186.74 | VI 6251.82 | 4416.97 | 1396.75 | -423.30 | 45.65 |
| 219 | 72 | FeI 6188.00 | VI 6216.35 | 3553.23 | 2066.35 | 339.51 | -396.36 |
| 220 | 84 | FeI 6188.00 | VI 6251.82 | 4280.94 | 1108.25 | -241.19 | 18.03 |
| 224 | 56 | NiI 6204.64 | VI 6251.82 | 4391.23 | 1869.13 | -739.26 | 105.03 |
| 227 | 62 | FeI 6215.15 | VI 6216.35 | 2826.97 | 2738.04 | -740.68 | 67.25 |
| 228 | 74 | FeI 6215.15 | VI 6251.82 | 4285.67 | 690.31 | -93.85 | 4.37 |
| 230 | 85 | VI 6216.35 | FeI 6226.73 | 8805.03 | -3491.99 | 1046.24 | -115.13 |
| 232 | 49 | VI 6216.35 | SiI 6237.33 | 7067.14 | -2706.02 | 1185.79 | -188.29 |
| 233 | 67 | VI 6216.35 | SiI 6244.48 | 6910.79 | -1760.62 | 522.44 | -54.71 |
| 236 | 57 | NiI 6223.99 | VI 6251.82 | 4427.37 | 1512.21 | -504.36 | 60.25 |
| 237 | 67 | FeI 6226.73 | VI 6251.82 | 4224.50 | 1716.74 | -561.76 | 64.16 |
| 238 | 98 | FeI 6232.65 | VI 6251.82 | 4444.99 | 594.25 | -75.02 | 3.16 |
| 239 | 80 | SiI 6237.33 | FeI 6240.66 | 5784.57 | -4004.60 | 4746.01 | -1323.72 |
| 241 | 79 | SiI 6237.33 | VI 6251.82 | 4652.83 | 577.31 | -83.43 | 4.16 |
| 244 | 60 | SiI 6237.33 | TiI 6258.11 | 5234.95 | -2260.85 | 3605.92 | -1150.10 |
| 245 | 59 | SiI 6237.33 | TiI 6261.11 | 4703.68 | -100.87 | 1375.47 | -488.66 |
| 249 | 83 | SiI 6244.48 | VI 6251.82 | 4716.94 | 676.72 | -117.71 | 6.99 |
| 252 | 88 | SiI 6244.48 | TiI 6258.11 | 5003.67 | -1820.76 | 4698.58 | -2025.39 |
| 253 | 63 | SiI 6244.48 | TiI 6261.11 | 4633.20 | 356.28 | 1646.00 | -816.49 |
| 255 | 95 | FeI 6246.32 | VI 6251.82 | 4378.48 | 440.32 | -39.23 | 1.17 |
| 256 | 71 | VI 6251.82 | FeI 6271.29 | 6383.44 | -715.40 | -106.41 | 55.41 |
| 257 | 64 | VI 6251.82 | MgI 6318.72 | 6352.97 | -1291.30 | 191.10 | 24.57 |
| 260 | 75 | TiI 6261.11 | FeI 6330.86 | 9186.18 | -3487.31 | 933.99 | -84.83 |
| 262 | 96 | MgI 6318.72 | CrI 6330.13 | 2964.81 | 3400.01 | -1143.57 | 109.63 |
| 264 | 47 | CrI 6330.13 | FeI 6330.86 | 6633.91 | -656.44 | -534.35 | 185.91 |
| 265 | 80 | CrI 6330.13 | FeI 6380.75 | 6037.16 | 1172.08 | -3537.36 | 1484.66 |
| 266 | 67 | FeI 6392.55 | SiI 6414.99 | 6480.93 | -1660.87 | -556.96 | 525.34 |
| 274 | 75 | FeI 6703.58 | SiI 6721.85 | 7317.80 | -2006.40 | 66.05 | 126.73 |
| 275 | 65 | FeI 6710.33 | SiI 6721.85 | 6467.06 | -1713.33 | 129.43 | 114.98 |